POLITECNICO DI MILANO

Dipartimento di Ingegneria dell'Informazione

Wilt oak trees detection using hyperspectral images with neural networks and GTI method

Relatore: Prof. Marcello Restelli

Tesi di laurea di:

Massimo Dell'Erba Matr. 734970

Anno Accademico 2009/2010

Abstract

In this work I proposed methods for detecting wilt oak trees. There were used images regarding Japanese Oak forests captured during summer and autumn of years 2007, 2008 and 2009, from airborne and from low-altitude.
Artificial Neural Network approach was the first adopted and obtained results were not reliable as expected from other past studies.
On the other hand, GTI method permitted of splitting into 2 subsets (wilt and healthy), the pixels of an image taking care also about autumnal characteristics of leaves, using reflectance graphs of each pixel in function of wavelength. 2 different strategies were followed: finding a static threshold with many observations or running an algorithm (MCC) to find a dynamic threshold. The second approach was better for both dark and subject to accentuated atmospheric effects images. Moreover it resulted effective also for other goals, like detecting wilt rice fields and classifying different grass species in a certain area.

Riassunto

In questo lavoro di tesi abbiamo sviluppato e valutato dei metodi per individuare e classificare caratteristiche di organismi vegetali (specie, presenza di malattie), a partire da immagini acquisite mediante tecniche di telerilevamento.

Immagini utilizzate

Le immagini raccolte sono di due tipi:

- da altitudine prossima allo 0 rispetto al livello delle piante da acquisire
- da un aereo alla quota di 1000 m

in entrambi i casi sono di natura iperspettrale, cioè presentano per ogni pixel lo spettro della radiazione in funzione della lunghezza d'onda che varia dal visibile (400nm) all'infrarosso (fino a 1000 nm)

Queste immagini possono direttamente essere usate per classificare i pixel oppure possono essere raffinate (ad esempio tramite funzioni di smooth), per eliminare il rumore e correggere disturbi derivanti dall'illuminazione scarsa e/o dall'angolazione non perfetta dello strumento al momento dell'acquisizione.

Approccio con le Reti Neurali Artificiali

Ci siamo occupati di classificare i pixel di immagini tratte da foreste di querce giapponesi. L'obiettivo era discriminare tra zone affette da Platipus Quercivora (un coleottero che si insinua nel tronco degli alberi bloccando il flusso di clorofilla).

Il primo approccio seguito è stato quello delle reti neurali artificiali, in particolare è stata adottata una rete multipercettrone con un layer nascosto.

La configurazione migliore prevedere 10 neuroni nello strato nascosto e l'utilizzo della sigmoide logaritmica come funzione di attivazione di tutti i neuroni.

Come riferimento abbiamo usato delle immagini precedentemente classificate e questo approccio si è rilevato di scarsa qualità in quanto molti pixel sono stati scorrettamente rilevati

Ovviamente, utilizzando immagini non raffinate si hanno più errori.

Inizialmente, le lunghezze d'onda acquisite, sono state interpolate col metodo dei minimi quadrati per avere una forma d'onda e poi usate come input alla rete neurale. Utilizzando funzioni ottenute mediante spline il risultato è leggermente migliorato anche se la qualità è rimasta troppo bassa per poter considerare tale approccio affidabile.

Inoltre, un ulteriore punto a sfavore delle reti neurali è rappresentato dall'eccessivo tempo computazionale.

Da questi risultati è quindi nata l'esigenza di sviluppare un nuovo metodo che portasse ad una miglior qualità della classificazione.

GTI Statico

Basandomi ancora sullo studio delle querce, il secondo metodo sviluppato è consistito in uno studio delle forme d'onda della radiazione in funzione della lunghezza d'onda per cercare di estrapolare informazioni sugli andamenti caratteristici dei pixel malati e di quelli sani. Analizzando circa un migliaio di pixel tratti da immagini diverse catturate in diversi periodi dell'anno, ho notato che per lunghezze d'onda comprese tra 500 e 700 nm i pixel malati hanno una radiazione che cresce più lentamente di quelli sani. Da questa osservazione è stato possibile ottenere una soglia che fosse in grado di dividere i pixel sani da quelli malati in base al valore della crescita nel suddetto intervallo (misurata come differenza tra la radiazione in 700 e quella in 500 nm). Questa è l'idea base del GTI (Growth Threshold Infrared) Statico.

Analizzando le immagini catturate in autunno inoltre, è stato possibile rilevare che le forme d'onda in quell'intervallo sono concave, a differenza di quelle analizzate in periodi non autunnali che presentano un andamento convesso sia nel caso sano che in quello malato. Quindi, per ottenere una classificazione efficiente è stato necessario un controllo iniziale delle natura del pixel, andando di fatto ad identificare tre insiemi di pixel: pixel sani, pixel sani e autunnali, pixel malati.

Tale metodo è stato poi esteso allo studio di risaie affette da un batterio e nella classificazione di diversi tipi di erba in un campo con buoni risultati. Di fatto quindi è stata trovata una soglia per dividere i pixel in insiemi per tutte queste specie.

Il problema maggiore di questa tecnica però, deriva dal fatto che la soglie trovate sono appunto statiche, quindi mal si adattano ad immagini catturate in un range di situazioni possibili (scarsa illuminazione, angoli di incidenza della luce solare o ancora, diversa qualità dello strumento di acquisizione). Nonostante le operazioni per raffinare le immagini iniziali, spesso non si raggiunge una qualità comparabile con quelle ottimali, quindi, per immagini catturate in condizioni molto diverse tra loro sarebbero necessarie più soglie, cosa del tutto infattibile considerando il troppo ampio ventaglio di casi possibili; è nata quindi l'esigenza di sviluppare un

ulteriore metodo che fosse in grado di adattarsi all'immagine presa in considerazione per poter agire in modo efficiente anche con immagini non ottimali per lo studio in questione.

GTI Dinamico

Per ovviare ai problemi elencati nella sezione precedente, ho seguito un altro approccio: quello degli algoritmi di clustering. L'idea alla base è stata quella di creare algoritmi in grado di adattarsi dinamicamente alle caratteristiche dell'immagine analizzata, trovando in modo efficiente le categorie dei pixel. Per i motivi appena espressi, questo modo di agire è stato denominato GTI Dinamico.

Il primo algoritmo sviluppato è il CC (Category Catcher), che, partendo da un insieme iniziale di valori (nel caso studiato i valori della radiazione negli intervalli ritenuti interessanti dall'esperienza del GTI Statico), è in grado di suddividerlo in due sottoinsiemi, pixel sani e malati nel caso delle querce. Un tale algoritmo però, per quanto utile per problemi in cui si sa in anticipo che si hanno solo due categorie da trovare, non è di molto aiuto ed anzi può portare a risultati altamente scorretti in tutti quei casi in cui non è noto a priori quante sono le categorie in cui suddividere l'insieme di dati iniziale. Quest'ultima considerazione rende anche superfluo il test con l'algoritmo K-means in quanto anch'esso pretende l'inserimento di un numero di categorie rigido come dato in ingresso. Quindi, partendo dal CC è stata presa definitivamente la strada che portava alla creazione di un algoritmo ad-hoc, come per la maggior parte dei problemi riguardanti immagini iperspettrali. E' stato allora sviluppato il MCC (Multiple CC), che riceve in input oltre all'insieme iniziale il numero massimo *n* di categorie in cui suddividere l'insieme e in output può fornire un numero di categorie che variano da 1 a *n*, quindi variabile e dipendente dai dati in ingresso. L'MCC è di natura istografica basato sulle distanze tra i valori dell'insieme di ingresso.

Conclusioni

Come espresso sopra, le reti neurali mal si prestano a questo studio e non è quindi una buona idea utilizzarle per motivi di sforzo computazionale e qualità dei risultati.

L'MCC si è dimostrato estremamente affidabile in quanto, studiando oltre alle querce anche risaie ed erba, ha rilevato correttamente il 15% dei pixel in più del CC, classificando correttamente il 96% dei pixel presi in considerazione da immagini note da ispezione umana. Essendo un metodo che si basa su dati sperimentali, è ovvio il non raggiungimento della perfezione. A volte il rumore dei dati rende le distanze tra le categorie scorrette.

Un'ultima considerazione da fare riguarda il fatto che, potendo fissare un numero *n* massimo di categorie, queste aumentano sempre più man mano che *n* aumenta. Per esempio, fissando *n=2* per l'analisi delle querce affette dal Platipus Quercivora, l'MCC, rileva correttamente due categorie, fissando *n=3* ne determina ancora 2 ma quando impongo *n=4* ne trova 3. Questo risultato è interpretabile dando un significato "fuzzy" agli insiemi creati; in particolare, si può dare un grado di appartenenza ad ogni insieme alla categoria sano o malato, ad esempio, per i sottoinsiemi agli estremi si può dire con certezza che sono sani o malati mentre per quello nel mezzo si può esprimere un certo livello di incertezza. Questo è del tutto lecito se si considera il problema del rumore nei dati che può rendere erronea un categorizzazione per alcuni pixel a cavallo tra un sottoinsieme ed un altro. Per le zone con un livello di incertezza si può quindi programmare una ispezione umana mentre per le altre no, il che snellisce di molto il lavoro dell'uomo. Questo discorso è ovviamente applicabile anche al caso delle risaie e dell'erba.

Fissare un valore *n* molto più alto rispetto a quanto ci si attende ha anche il significato di ottenere una classificazione più raffinata. Per esempio, se si pensa che in prato ci siano due specie diverse di erba si potrebbe fissare *n=6* e se si ottenessero 4 sottoinsiemi allora si sarebbero individuate anche le sottospecie.

Sviluppi futuri

Al fine di migliorare la qualità delle immagini iperspettrali e di poter investigare aree più ampie con meno acquisizioni, vari progetti sono in corso per trovare delle soluzioni. Una di queste è di matrice italiana ed è un satellite di nome PRISMA s, sviluppato dall'ASI (Agenzia Spaziale Italiana), che presenta un sensore iperspettrale molto raffinato.

Il miglioramento continuo degli strumenti di acquisizione porterà sempre più ad avere immagini migliori e più facili da studiare.

Summary

1 – Introduction

The detection of features about big geographic areas can represent a crucial point to safeguard and monitor the environment. Remote sensing and machine learning techniques are a possible combination to do this efficiently. From the origins of this approach there were studied and tested a lot of methodologies with fluctuating results. Thus, there is still a wide range of applications without a reliable method to face up to the problem. One of these is presented in this thesis work.

1.1 – Motivation and goal

An efficient detection of features regarding vegetables represents a crucial point to monitor the situation of giant vegetal areas. Such features involve diseases and settlement of new species. Create thematic maps with pointed out different properties of each portion of the studied area is the final target when someone is about to conduct a work like this.

In particular simple human inspection could seem a solution but can be easily understood that this method cannot be adopted when big areas are considered. Moreover the percentage of error in detection would be too high. In this context, automatic methodologies are highly welcome.

The problems here debated is finding a reliable procedure to detect oak trees affected by Platipus Quercivora (Apx. 1). This beetle is diffused mostly in Japan and north America. Without a careful monitoring of subject areas, epidemics could rise. Thus, it is very important to develop instruments in order to prevent the death of a lot of trees.

1.2 - Followed approach

First, it was chosen to use as raw material remote sensing data, in particular airborne and low-altitude hyperspectral images of Japanese (precisely Syonai Shinrin district), oak forests captured during august 2008 with modifications of data acquired (paragraph 3.3), in order to attenuate disturbing effects, like, for example, atmospheric ones, and June – August 2009 with not modified data.

After the acquisition and refinement of images, there were adopted two main methods: Artificial Neural Networks (ANNs) and Clustering (GTI).

ANNs did not give good results since the error in detection was elevated, thus there was not any improvement in efficiency if compared with existing methods explained in the next Chapter.

Regarding the other method used, GTI (Growth Threshold Infrared), there were developed two different methods:

- Development of a static procedure based on a fixed threshold for discriminating between healthy and wilt oak trees
- Development of an algorithm to do classifications by changing the threshold dynamically.

As said before, the target of this work was the detection of wilt oak trees, in order to promptly understand quickly if there is an epidemic. Moreover, it will be clear how GTI in particular can be used also for other vegetables for detecting diseases or classifying different species or properties [1].

Fig. 1.1 and Fig. 1.2, show examples of wilt oak trees. Not always it is possible with eyes to discover wilt trees (even for autumn tint leaves), so in such cases it is necessary a study like the one described in this thesis.

Fig. 1.1. Oak forest with eye-visible wilt oak trees

Fig. 1.2. Oak forest with possible not eye-visible oak trees

1.3 – Thesis structure

The work is presented with the following pattern:

- Chapter 2 overviews the state of the art in remote sensing studies with a particular focus on the aspects discussed in this thesis. In particular there are explanations about the kinds of images used, indexes to detect vegetation and methods adopted in the past to solve the problem here debated
- Chapter 3 is focused on the image acquisition. It talks about the differences between airborne and low altitude sensors and ways to memorize and refine pictures
- Chapters 4 and 5 present ANNs study showing what data are used as input, characteristics, limits and reached results
- Chapter 6 talks about Static GTI that is a rule-based approach which permits, starting from a fixed threshold, to split the initial set of pixels in different categories
- Chapter 7 is about Dynamic GTI. Differently from Static GTI, here are presented algorithms that are able to dynamically adapt to image to classify
- Chapter 8 shows a panoramic of obtained results and future work

2 – State of the art

In this Chapter are presented characteristics, merits and defects of the existing methods applicable to the problem discussed in this thesis work.

2.1 - Currently used images

Multi-spectral imaging [1] is a technology originally developed for space-based imaging. which can capture light from frequencies beyond the visible light range, such as infrared.

Multi-spectral images are the main type of pictures acquired by Remote sensing radiometers. Usually satellites have 3 to 7 or more radiometers. Each one acquires one digital image (in remote sensing is called scene), in a small band of visible spectra (that is from 0.4 μm to 0.7 μm), going up to infra-red wavelengths (from 0.7 μm to 1.0 or more μm). Multi-spectral images with more numerous bands, finer spectral resolution or wider spectral coverage are called hyperspectral.

Moreover, for both hyperspectral and multispectral images, there are not only satellites as acquisition media. In particular there are airborne and low-altitude sensors too. Low altitude sensors have the advantage to present a high resolution but they cover a small area. Satellites have rough resolution, high cost, but they cover a giant area with a single image. Aiborne devices are in the middle. Research work in this field has the main goal to obtain satellite sensors with a resolution similar to the airborne one.

In order to be more precise, below there are the principal characteristics of multispectral and hyperspectral devices:

Multispectral

- Low spectral resolution
- Band width of 0.1 or 0.2 μm

Hyperspectral

- High spectral resolution
- Band width of about 0.01 μm

Hyperspectral remote sensors collect image data simultaneously in dozens or hundreds of narrow, adjacent spectral bands. In this way it is possible to have an almost continuous spectrum for each image cell.

Hyperspectral images are produced by instruments called imaging spectrometers which are based on two disciplines: spectroscopy and remote imaging.

Spectroscopy is the study of light that is emitted by or reflected from materials and its variation in energy with wavelength, moreover this technology deals with the spectrum on sunlight that is diffusely reflected from the materials at the Earth's surface. A spectroscopic study is done by a spectrometer. A prism into this device splits light into many adjacent wavelength bands and the energy in each band is measured by a separate detector. With a lot of detectors (also thousands), the width of narrows can be of about 0.01 μm over a wide wavelength range (usually from 0.4 to 2.4 μm).

Remote imagers instead, are designed to focus and measure the light reflected from many adjacent areas on the Earth's surface; sequential digital images are made in consistent geometric pattern as the sensor of platform moves and subsequent processing is required to assemble them into a unique image. Recent advances in these areas have allowed the design of imagers that have spectral ranges and resolution comparable to ground based spectrometers.

2.2 - Common vegetation indexes

Vegetation indexes on images arriving from satellites, airplanes or low altitude are very important and very used for the monitoring of the situation of entire areas. Those indexes are based on the combination of two or more spectral bands. They are made through algebraic combination of reflectance [2, 3] (Apx. 2), in red and infrared spectral interval, because vegetation has a great interaction in these points of the spectrum.

Chlorophyll in most part absorbs incident electromagnetic radiation, mostly in visible part of the spectrum. The result is a spectral signature with a low reflectance, in blue, red and high in near infrared because of the diffusion of energy from internal parts of leaves. The contrast between red and near infrared, permits to distinguish very well vegetation in images. There were defined many indexes [2,3] to manage this information, as showed below.

A very used index is NDVI (Normalized difference vegetation index), which can be derived as:

$$NDVI = \frac{r_{IR} - r_{Red}}{r_{IR} + r_{Red}} \quad (1)$$

With r it is indicated the reflectance. If an image is analyzed with the NDVI, the result is the same image in grayscale which is useful for analysis. This index is dependent from ground effects. Another index is NDGI, defined as:

$$NDGI = \frac{r_{Green} - r_{Red}}{r_{Green} + r_{Red}} \quad (2)$$

(1) and (2) are effective for different kinds of vegetation. A commonly used strategy is the following:

- Obtain *NDVI* values
- If these values are too similar and thus not usable to classify, than compute *NDGI*

These two indexes can be combined together to form the SD index, which reduce the dependency from bands of wavelengths:

$$SD = NDVI + NDGI \quad (3)$$

Moreover there is another index particularly able to detect oak trees for images captured in optimal conditions NWI (Normalized Wilt Index):

$$NWI = -NDGI \times SD = -NDGI \times (NDVI + NDGI) \quad (4)$$

where

$$-NDGI = \frac{r_{Red} - r_{Green}}{r_{Red} + r_{Green}} \approx \frac{dR(\lambda)}{d\lambda} \mid \lambda = \lambda_{Red} \quad (5)$$

$$NDVI + NDGI = \frac{r_{IR} - r_{Red}}{r_{IR} + r_{Red}} - \frac{r_{Red} - r_{Green}}{r_{Red} + r_{Green}} \approx \frac{d^2R(\lambda)}{d\lambda^2} \mid \lambda = \lambda_{Red} \quad (6)$$

In NDGI-NDVI space it is possible to define two other indexes through two dimensions: in the first of these a scale of coloration, so we have the TI (Tint index); instead in the second axis (orthogonal to the first), we have the WI (Whitering Index). To calculate these values it is necessary, in NDGI-NDVI space, the data projection onto the whitering and/or tint axis.

2.3 – Focus on vegetal studies

The study of properties about vegetation is performed mostly using indexes showed in the previous paragraph [4]. The main problem about this approach is the low adaptability; in fact, the same image captured in different conditions (i.e. solar illumination), present for the same pixels two different values of each index. Sometimes the difference is too high and this leads to opposite conclusions. Since very often the work has to be carried on with many kinds of images (Chapter 3), and that techniques of refinement are not able to perfectly uniform pictures, indexes based procedures are not reliable. To improve the situation, there were tried to fix characteristic values of indexes to individuate properties (i.e. oak trees affected by Platipus Quercivora [4]), but in many cases [4,5,6] big fluctuations from these values gave a lot of doubt about the quality of found results. Obviously, indexes present the same problem even for other vegetation [7].

ANNs approach is also used for oak trees [4, 8, 10, 11, 12, 13, 14, 15] but even in this case results are too dependent from conditions in which the image was captured. Even with well captured pictures this method could present a high percentage of wrong classifications. Moreover, the computational effort is huge. It is used to try to adopt first ANNs because of their simplicity and then change method once viewed the low quality of the result.

ANNs can be a valid alternative respect to indexes in roughly classify different materials on a captured picture. For example, distinguish between vegetation and roads. For problems which request a more refined classification (i.e. finding wilt and healthy trees), this approach is not reliable. Fig 2.1 shows an example.

Clustering techniques have been used too. Usually ad-hoc algorithms are used [16, 17, 18, 19, 20, 21, 22, 23, 24], because existing ones are not appropriate for the classification problem to solve. Of course the reliability depends on the asset of the developed algorithm. In particular, two different approaches were followed in research works:

- Finding discriminating features through a single algorithm running and applying them to every future set of data (obviously regarding the same thing).
- Applying the algorithm for every set of data. This approach is reliable for a large variety of fields, so it can be considered the most important one to start the research work.

One general problem of clustering algorithms is the big computational effort.
Moreover, the major drawback about clustering approach is that every algorithm presents some weakness in detection. Often algorithms' results are too discordant to each other and everyone presents blunders (accuracy less than 85%), for every kind of material studied [25] as shown in Figs. 2.2, 2.3a and 2.3b.

Another problem is the following: sometimes data that has to be classified are very closed to the boundary between one category and another one (in our case, the boundary between wilt pixel set and healthy one). In this case the data will be assigned to a set without considering problems about the noise in the data that can modify some characteristics of them changing their position from one side to the other of the border. These situations are uncertain and because of the noisy nature of experimental data, sometimes it is not possible to completely remove the problem. Thus, these cases have to be considered because assigning a precise category to some data could represent a mistake. Creating another set for uncertain data can represent a solution. Since these data in general represent a small part of the entire set to study, a human inspection to establish the real nature of them is possible. About oak trees (and not only), an approach like this which is able to consider doubtful data does not exist.

In some situations, the study can be carried on improving at each step the accuracy. For instance, in order to have a preliminary idea in short time it is used to calculate indexes first. Then, once

obtained the entire thematic map, it is already possible to obtain some conclusions even if in general not very accurate. The second step is to use another method, more reliable than indexes, which can give as output a second thematic map, more accurate than the first one. However, depending on the kind of the work that has to be performed, it is not always possible to apply the second step because it is generally slower and sometimes there is not enough time (some applications could request very fast results, like the monitoring of an area affected by a fire). In the work presented in this thesis there are not strict time constraints because the observation of affected oak trees can be done once every two days, so there is enough time to obtain maps, but, as explained before, existing methods do not present an appropriate accuracy. Moreover, even if not crucial, finding a faster method can help the analysis and always represent an important improvement. Thus, from these statements started the idea to conduct this thesis work.

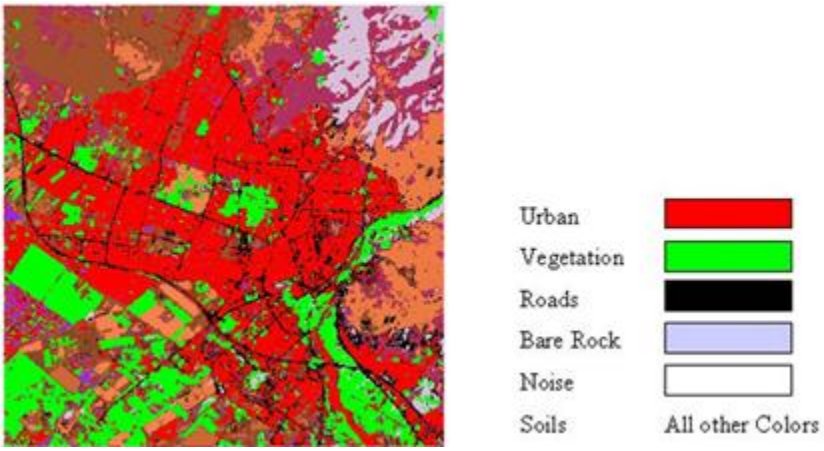

Fig. 2.1. An example of classification using ANNs, the accuracy is high (98.3%), but trials to distinguish different kinds of vegetation had lower accuracy [25]

Fig. 2.2. An image to classify

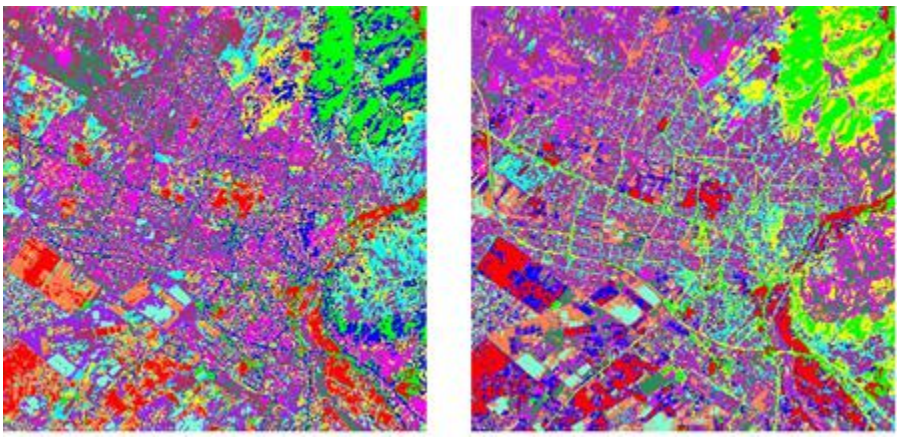

Fig. 2.3. (a) Classification with Isodata algorithm; (b) Classification with K-means

3 – Acquisition and refinement of images

Here are treated instruments to catch hyperspectral images and methods to optimize them in order to make less difficult the study.

3.1 – Devices and software used

In order to obtain low-altitude [6] hyperspectral images for having ground references (as explained in 1.1), it was used Specim. ®.Imspector-V10 (Fig. 3.1) which has these main features:

- Spectrum range: 400 - 1000 nm
- Resolution of spectrum wavelengths captured: 5 nm
- Able to take 30 fps.
- Number of bands: 121
- Number of pixels for each image: 484
- Spatial resolution (Apx. 3) < 40 μm

To obtain reliable data it is necessary to have spectral characteristic of a well known surface (Fig. 3.2), that is the standard reference [9]:

Fig. 3.1. Imspector-V10

Fig. 3.2. View of standard reference into a vegetation zone

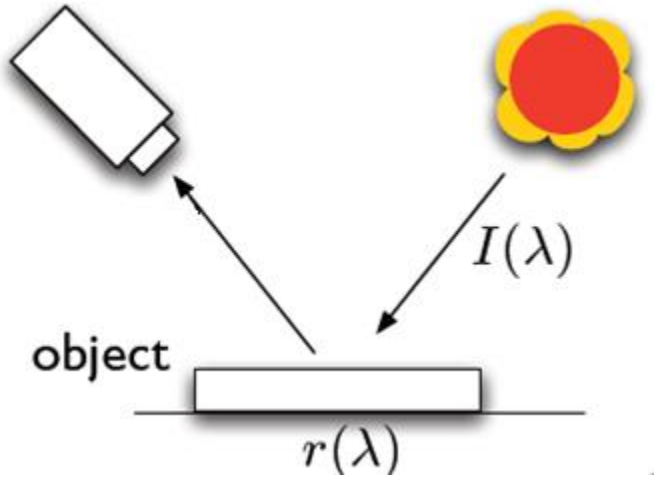

Fig. 3.3. Low-altitude radiance acquisition

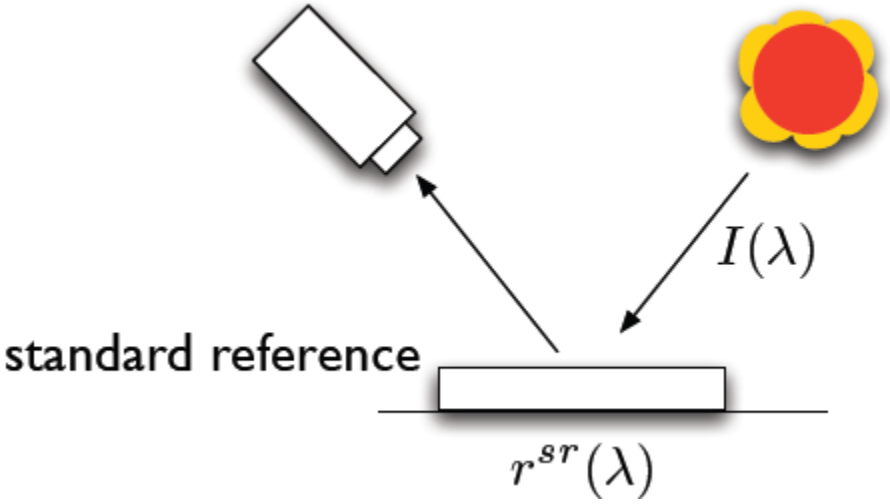

Fig. 3.4. Low-altitude radiance acquisition for standard reference

With this element it is possible acquiring all interesting features (Figs. 3.3 and 3.4).

L is the radiance, r is the reflectance, sr stands for standard reference, λ the wavelength and I is the illumination. Having this information is possible obtaining reflectance of each pixel of interesting surface (for example of parts with vegetation from Fig. 3.2):

$$L^{sr}(\lambda) = r^{sr}(\lambda) I(\lambda) \tag{7}$$

$$L(\lambda) = r(\lambda) I(\lambda) = \frac{r(\lambda)}{r^{sr}(\lambda)} L^{sr}(\lambda) \tag{8}$$

$$r(\lambda) = r(\lambda) \frac{L(\lambda)}{L^{sr}(\lambda)} = r^{sr}(\lambda) \frac{S(\lambda) DN(\lambda)}{S(\lambda) DN^{sr}(\lambda)} = r^{sr}(\lambda) \frac{DN(\lambda)}{DN^{sr}(\lambda)} \tag{9}$$

DN is the digital number derived from radiance (a good mechanism to do this is explained talking about AISA images) and S is the first derivative, in function of wavelength, for DN $-$ L graphs in function of wavelength.

Airborne hyperspectral images, were captured by AISA® view device (developed by NASA, in Fig 3.5 is possible viewing the structure), with these characteristics (Fig. 3.6 shows how data are acquired):

- Spectrum range: 400 - 2500 nm
- Resolution of spectrum wavelengths captured: about 8.18 nm
- Number of bands: 195
- Samples: 324
- Lines: 1792
- Number of pixels: Samples x Lines
- From altitude of 1 km the spatial resolution along the track is 1 m

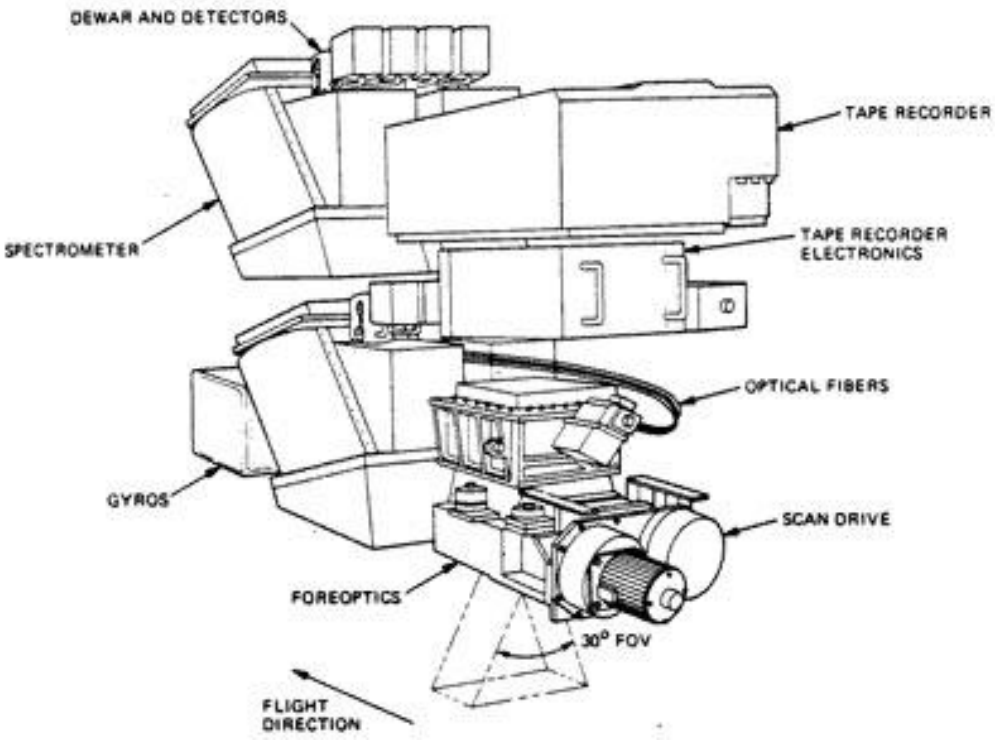

Fig. 3.5. Structure of Aisa view detector

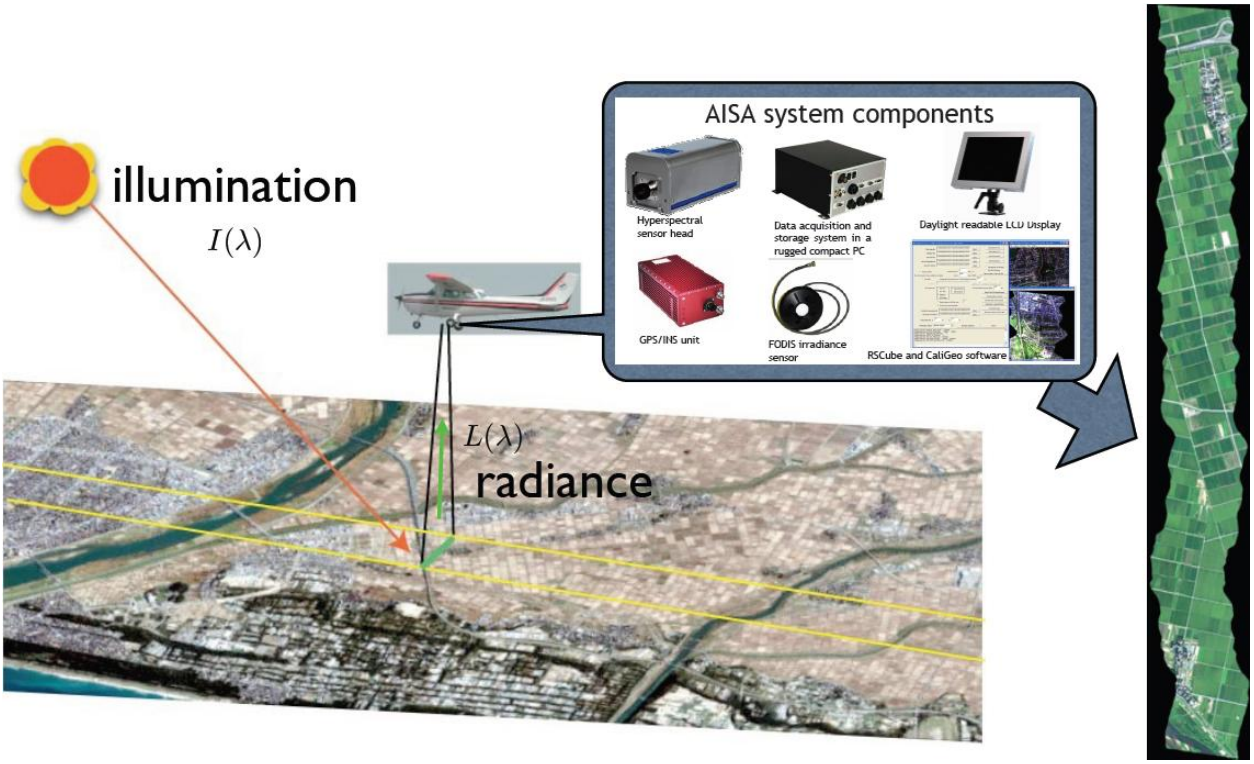

Fig. 3.6. How AISA system captures data

Thus, the hyperspectral sensor (with also irradiance one, which gets electromagnetic radiation at observed surface per unit of area), is able to capture radiance directly from the observations with the help of solar illumination. Position of pixels acquired is taken by a GPS unit. Data are then managed by an acquisition and memorization device. Moreover, in order to have real time information regarding observed area to make a preliminary analysis and to choose what is useful acquiring, Caligeo® software is often used for visualizing just caught images. The first work that AISA system does with images is the transformation of radiance (in Fig. 3.7 indicated in function of wavelength), into digital numbers, regarding bands acquired for each pixel (Fig. 3.8):

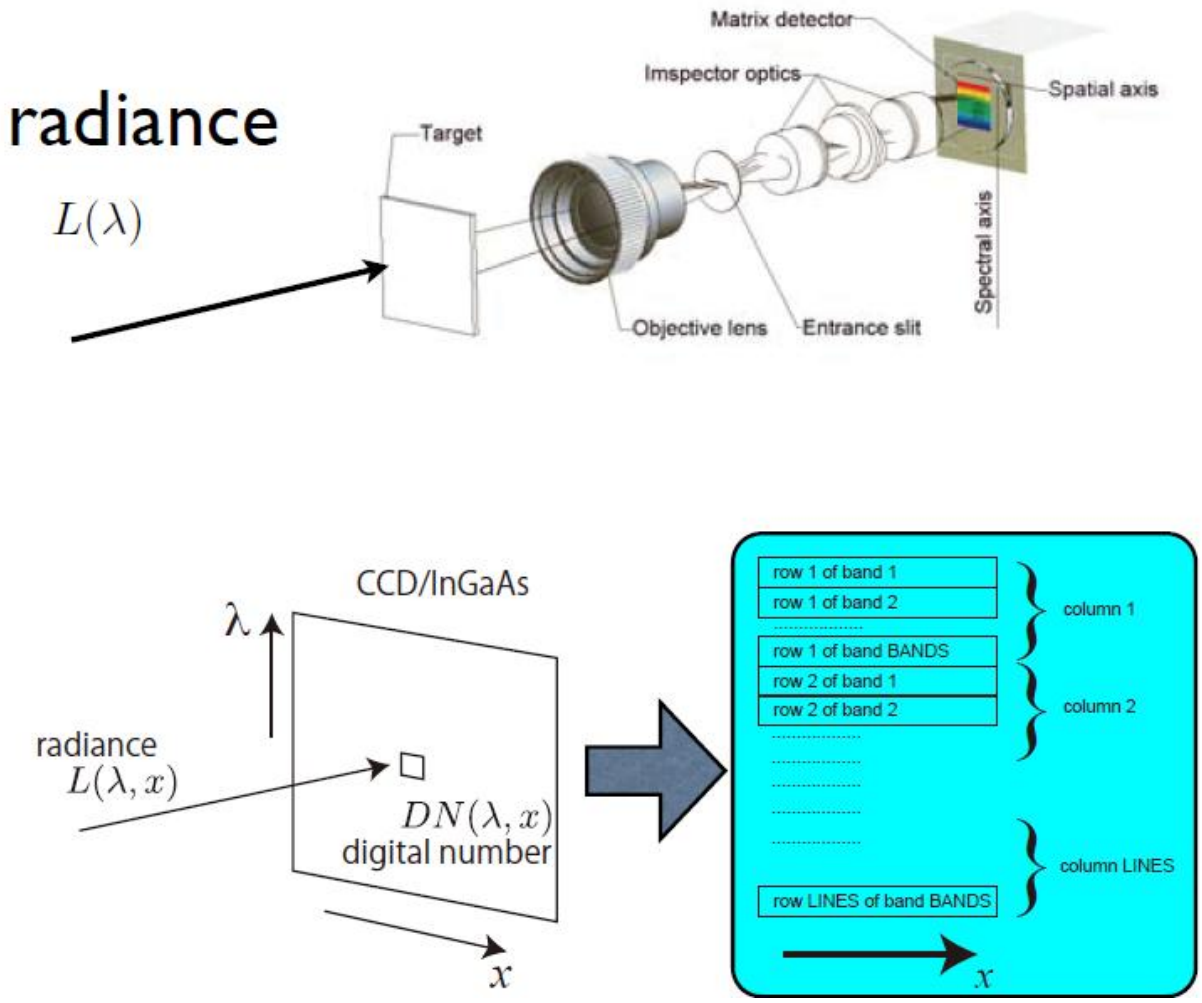

Fig. 3.7. Passages to obtain Digital numbers that represent radiance and style of memorization

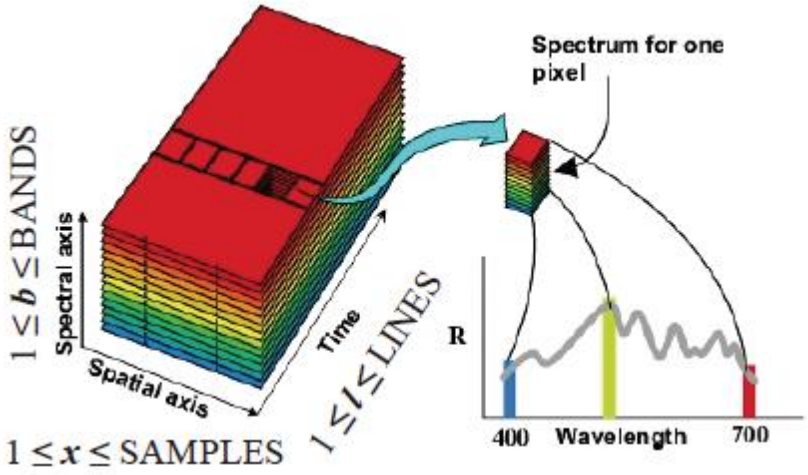

Fig. 3.8. Information acquired by AISA

Radiance data were then saved into disk in BSQ format. BSQ (Band SeQuential) permits a memorization in the format Colons – Rows – Bands where the third parameter indicates a vector of wavelengths. BSQ was chosen because it permits a quick access to spatial information (X-Y).

After this work, in order to make simply accessible images data and information about them, it is useful saving information in a standard format. For this study it was used ENVI format which has these two main components:

- Binary radiance data file
- Header file which contains attributes (features of captured image and device used to do this)

Fig. 3.9 and 3.10 show example of, respectively, data and header files:

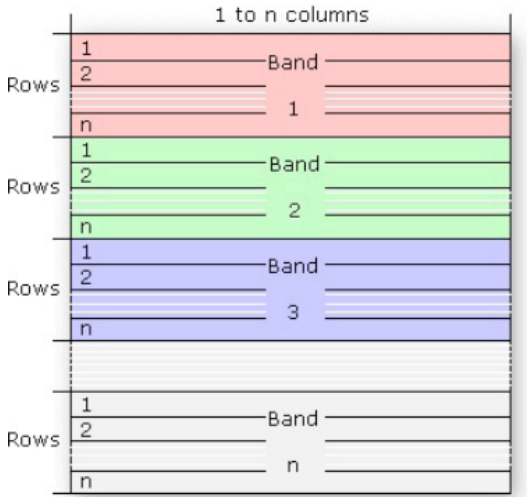

Fig. 3.9. Data file saved in BSQ format

```
ENVI
description = {
  Create New File Result [Thu Jun 18 16:45:21 2009]}
samples = 2798
lines   = 456
bands   = 195
header offset = 0
file type = ENVI Standard
data type = 12
interleave = bsq
sensor type = Unknown
byte order = 0
map info = {Transverse Mercator, 1.0000, 1.0000, -75968.7500, -125532.2500,
1.5000000000e+000, 1.5000000000e+000, , units=Meters}
projection info = {3, 6378137.0, 6356752.3, 40.000000, 140.833333, 0.0, 0.0, 0.999900,
Transverse Mercator, units=Meters}
wavelength units = Unknown
wavelength = {
  401.019989,  409.209991,  417.399994,  425.589996,  433.790009,  442.250000,
  450.820007,  459.380005,  467.950012,  476.510010,  485.070007,  493.640015,
  502.200012,  510.760010,  519.330017,  527.900024,  536.460022,  545.049988,
  553.890015,  562.809998,  571.710022,  580.630005,  589.539978,  598.440002,
  607.359985,  616.270020,  625.179993,  634.090027,  642.979980,  651.820007,
  660.669983,  669.520020,  678.359985,  687.210022,  696.070007,  705.049988,
  714.049988,  723.049988,  732.059998,  741.059998,  750.080017,  759.200012,
  768.340027,  777.479980,  786.630005,  795.770020,  804.909973,  814.059998,
  823.190002,  832.320007,  841.450012,  850.580017,  859.710022,  868.830017,
.....
.....
```

Fig. 3.10. Example of Header file

Here it is useful an explanation regarding some parameters not viewed before in the presentation of main features of AISA system.

- Header offset is the number of bytes into the file where the raster data begins, typically is 0
- Byte order is 1 for data file requiring data to be byte swapped to be used on Intel/Motorola hardware
- Data type is the kind of each pixel values into the dataset, here there were used 2 bytes unsigned integers
- Map info determines the coordinates of upper left corner of image and the pixel size
- Map projection is a vector which contains values for representing on a plane (in 2 dimensions), Earth images taken from airborne

- Wavelength is a vector with all wavelengths (in nm), captured and memorized for each pixel (in presented case, there were taken 195 values, that is the number of Bands)

In order to describe an image some of these parameters (or variants too), are necessary, but in general not all of them because sometimes it is possible to get a parameter observing the others. Together with other characteristics presented in explanation of AISA features, the only strictly necessary parameter above is data type. The others may become compulsory for particular studies, depending of the target of research; but in general, obviously, the more the parameters the simpler is the work.

Regarding map info is better saying more. Fig. 3.11 shows map info vector of Fig 0.12:

```
map info = {Transverse Mercator, 1.0000, 1.0000, -75968.7500, -125532.2500,
1.5000000000e+000, 1.5000000000e+000, , units=Meters}
```

Fig. 3.11. Map info vector

Transverse Mercator (Fig. 3.12), is a coordinate system for 2 dimensional images based on grid description. It is used to localize areas on Earth surface but is different from latitude and longitude method.

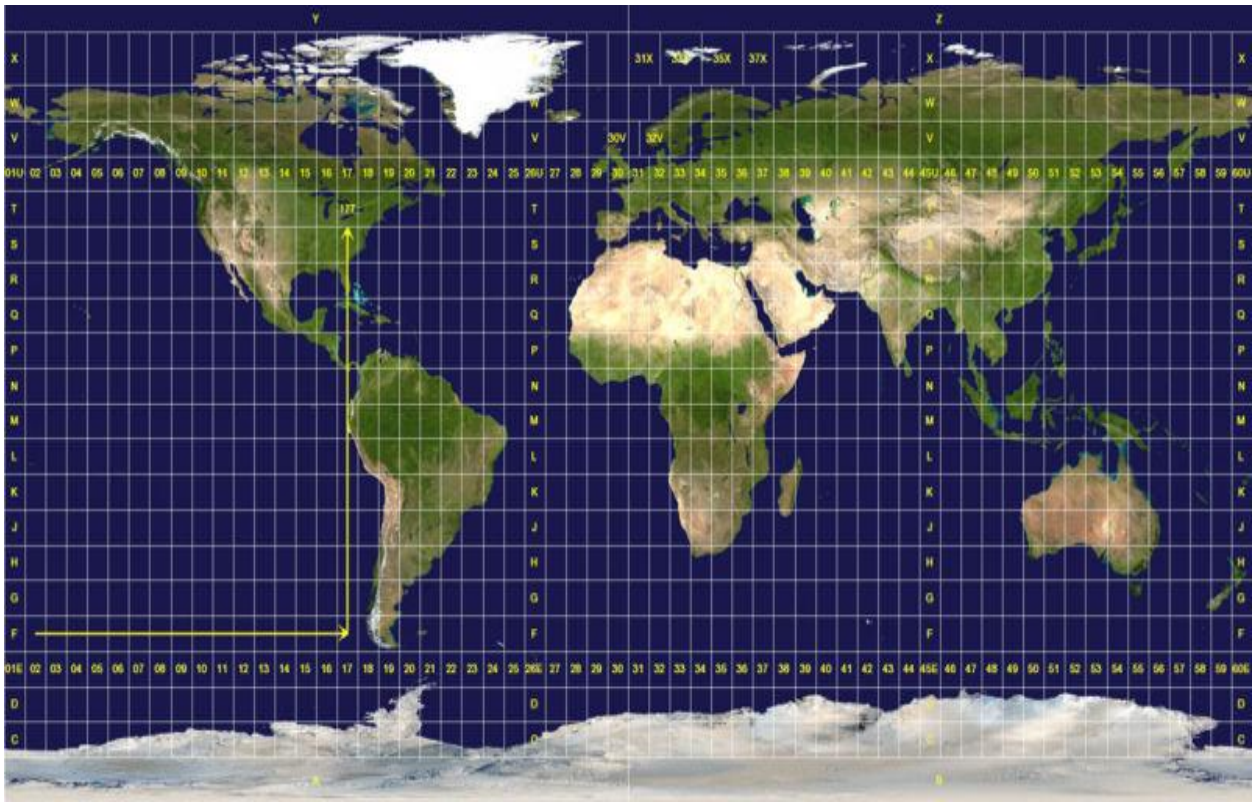

Fig. 3.12. UMT (Universal Transverse Mercator), grid

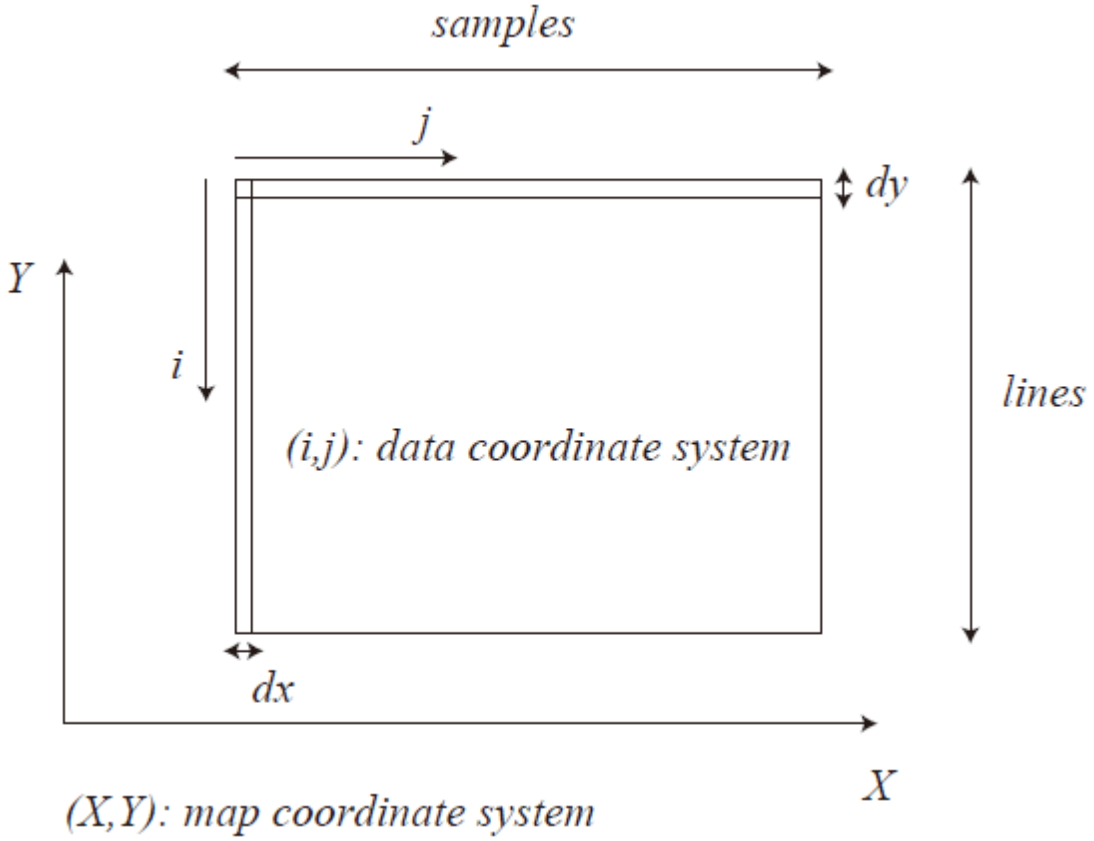

Fig. 3.13. Meaning of Map info numeric parameters (the rectangle represents a generic image)

After coordinate system, there are six values, calling them, in order of comparison in vector, *j*, *i* *X*,*Y*, *dx*, *dy*, is possible, looking at Fig. 3.13, their meaning.

All measures are reported in Meters.

Finally, starting from radiance values, to obtain reflectance ones is necessary following the proceedings explained in Fig. 3.14:

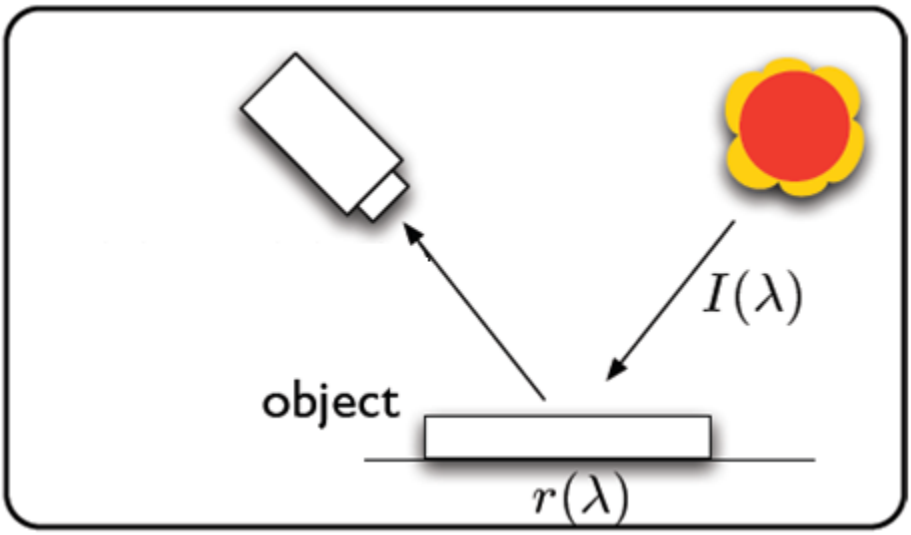

Fig. 3.14. Scheme of acquisition useful to get reflectance, similar for low-altitude images, but here is different the used device and the altitude (higher)

$$L(\lambda) = r(\lambda)I(\lambda) \qquad (10)$$

Inverting the presented formula (equal to the low-altitude one), it was possible obtaining reflectance values. But these data about reflectance were not very good for conducting a precise study, so they had to be refined.

Another used instrument was the Asd Inc ® Fieldspec, to capture spectrum information (ground references), about a precise and small area (Figs. 3.15 and 3.16), in order, for example, to make confrontations with spectrograph to test reliability of data acquired.

Fig. 3.15. Asd Inc ® Fieldspec

Fig. 3.16. Asd Inc ® Fieldspec plug to capture information about one precise region

About the software, it was used Matlab ® to do images elaboration and catching information starting from them. Furthermore, for having an initial overview of each picture before treatment it was used Geomatica ®.

3.2 – NDVI images

Sometimes, it was not simple to understand the difference between areas with plants and not; so an useful instrument to detect areas with plants was used, the NDVI index. Starting from the original airborne image (without any optimization), there were three steps to follow:

- Obtain reflectance values, for each pixel and for significant wavelengths in Near-Infra-Red and Red range (in this case there were chosen values respectively of 750 and 670 nm)
- Calculate NDVI index with (1) for each pixel of the image
- Introduce a threshold to better discriminate between vegetables and other materials

Below it is possible to observe an example through Figs. 3.17a and 3.17b:

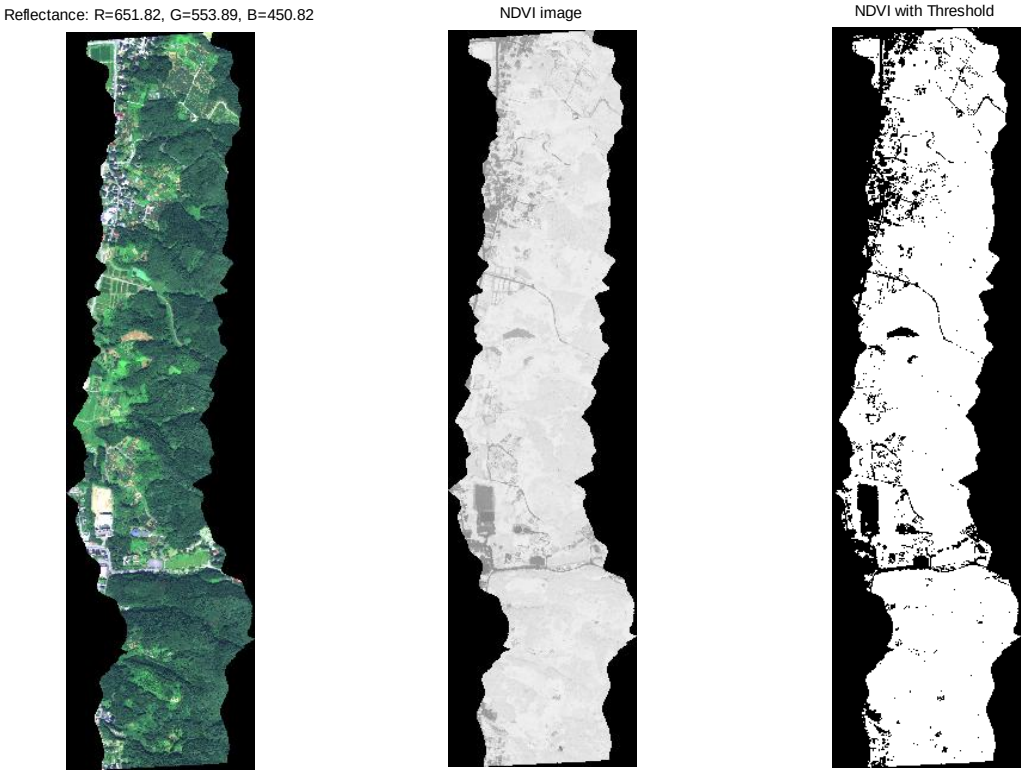

Fig. 3.17. (a) NDVI image after a threshold of 0.6 (vegetation in white, not-vegetation in black); (b) NDVI image; (c) NDVI with threshold of 0.4

It is important to say that the threshold is a value between 0 and 1. The higher threshold the more not-plant zones are discovered, but a very high value often causes errors in detection. Values from 0.4 and 0.6 are often good. The functioning of this system is the following: NDVI of each pixel is compared with the threshold. If the threshold is exceeded than that pixel represents a vegetation area (colored in white in Fig 3.17c), otherwise it is a not-vegetation one (colored in black).

3.3 – Values of reflectance

As said in 0.1, 2008 data about reflectance were modified in order to obtain a more suitable set of points, less subject to atmosphere, solar rays and also instrument features (Apx. 4, 5, 6). In this paragraph it is explained a method to find good reflectance values starting from the original hyperspectral radiance image; in particular is proposed the Calibration Hyperspectral Image method. It uses linear regression of the form:

$$y = ax + b \qquad (11)$$

where, for each pixel, x indicates the observed radiance spectrum in a relevant range (in our case 400 – 1000 nm), y ground references values in the same range of x (as the absolute values of the average between wilt and healthy oak trees), a and b are slope and intercept vectors of the regression line, respectively. In particular, a can be seen also as slope vector accounts for atmospheric transmittance differences and spectral shifts caused by the instrument and b represents the offset of radiance for each band induced by atmospheric path radiance. So, starting from x and y, it is possible to find a and b using a method which fits a generalized linear model using a particular distribution (in this case the Normal one), and after obtaining the fitting points (reflectance values), to have the final function like the one below (Fig. 3.18):

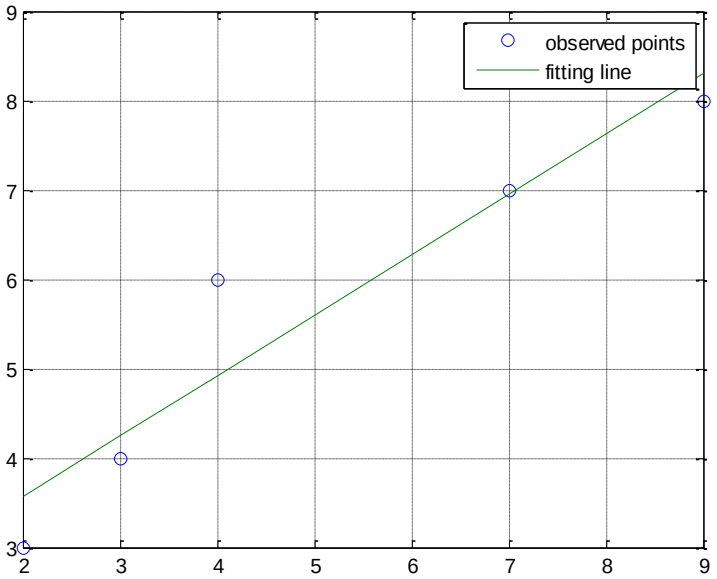

Fig. 3.18. Linear regression fitting method

It is important to say that jagging of ordinates of original observed points (blue circles in Fig. 3.18), it is caused mainly by disturbs mentioned before, thus, a linear regression model captures in general the most part of interesting data permitting to have a higher Signal to Noise Ratio (SNR). Using such method on an entire image is very long and occupies a lot of memory space, but it represents the best compromise between quality and speed. In order to obtain optimized reflectance values it is necessary to have also the sun incidence angle and more data about the radiance of each pixel, that for the most of images are not available (Apx. 7).

3.4 – Application of Calibration Hyperspectral Image method

Below it is described an example of application of Calibration Hyperspectral Image method for an image captured during August 2009. The radiance image is presented here (Fig. 3.19):

Fig. 3.19. Initial radiance image

Another important data for conducting the calculus is represented by the ground reference. In this case were captured standard references, regarding asphalt, orange and white sheets. Applying an average between these three radiance spectra, it was possible to obtain a good response and it is therefore possible to use the obtained values as ground reference (Fig. 3.20).

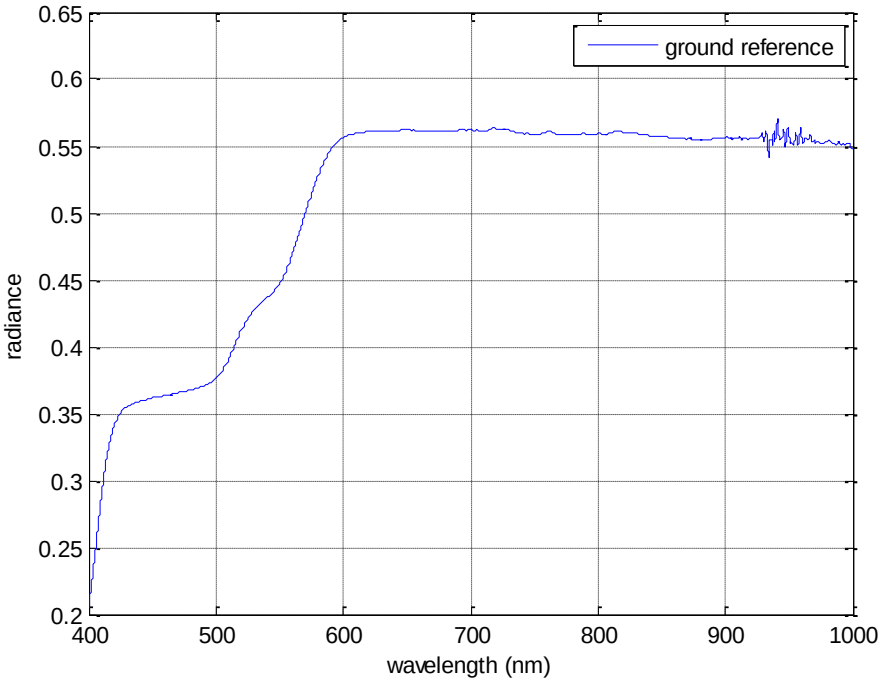

Fig. 3.20. Radiance spectrum of ground reference

In Figs. 3.21 and 3.22 are presented spectra of radiance and reflectance of a single pixel of Fig. 3.19.

The shape of the radiance spectrum is similar to the one about reflectance but the last mentioned has higher values mostly in visible range.

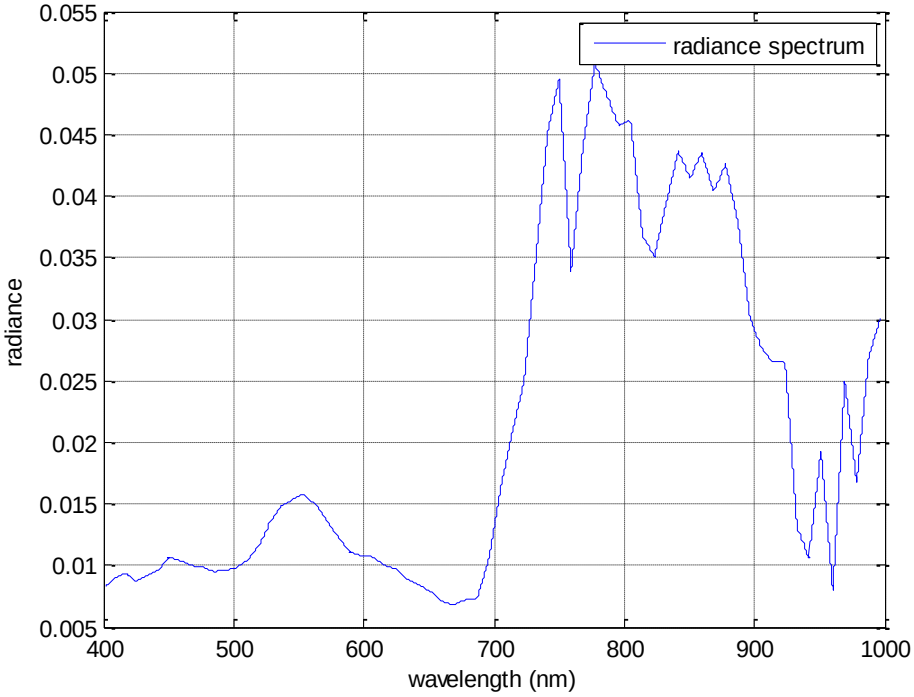

Fig. 3.21. Radiance spectrum of observed pixel

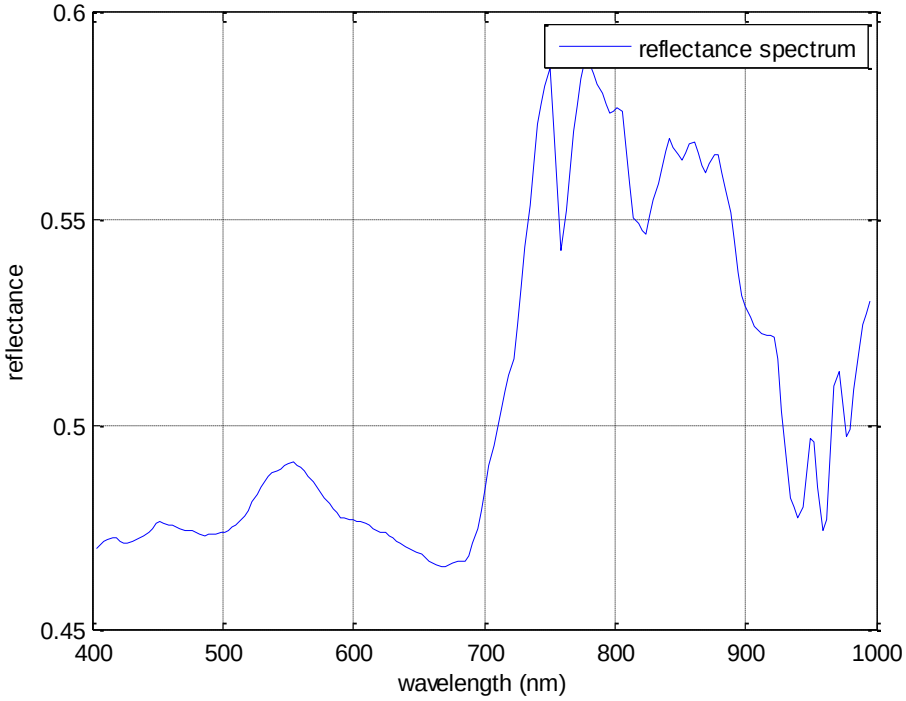

Fig. 3.22. Reflectance spectrum of observed pixel

4 - A first approach, ANNs

In this Chapter it is first discussed how to prepare hyperspectral data to be the input of an ANN. Then, characteristics and obtained results of ANNs approach are shown.

4.1 - Ground references

Fig. 4.1 shows a part as example of reflectance graphs for ground references chosen:

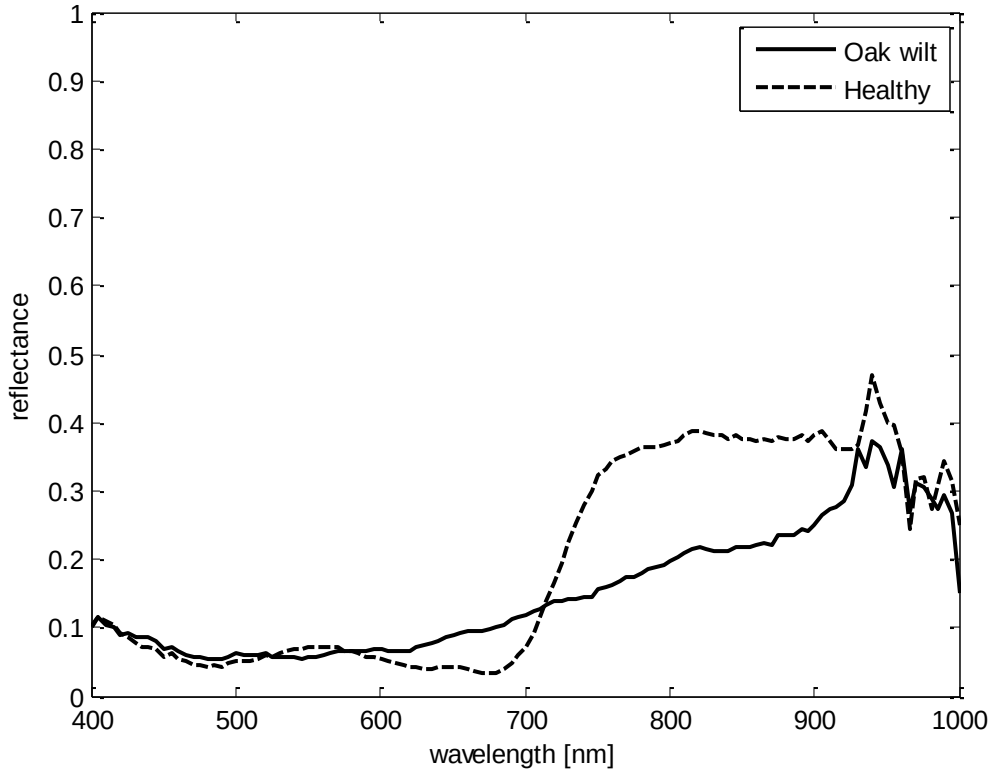

Fig. 4.1. Reflectance graphs for ground references, in function of wavelength

Data were captured during autumn 2008. This data were very useful during this work because they were used for classification of pixels (ground references represent trusted data). To obtain these data were captured low-altitude hyperspectral images [4], in order to obtain precise signature of interesting features.

4.2 - Hyperspectral image

The following hyperspectral image (Fig. 4.2), shows a part of a Japanese oak tree forest (September 2008):

Fig. 4.2. An optimized reflectance hyperspectral image of an oak forest

This picture is different from the original one (captured from the airborne); in fact, it was modified, in order to obtain optimal reflectance values, through the reduction of disturbing elements, like atmospherics, solar and regarding sensor gain and offset (Apx. 4, 5, 6). Moreover for each pixel there are reflectance values of the spectrum (Apx. 2).

From this zone, it was possible the zoomed observation of a precise area R, selected as a choice of an expert. Once caught R, the result was another image which represents the zoomed one (Fig. 4.3):

Fig. 4.3. A zoomed area of Fig. 2

From R was selected one pixel P1 (the red point of Fig. 3), with the goal of studying it to understand if it represents a zone with wilt oak trees or not. Usually, hyperspectral images are the most used for remote sensing studies [2, 5]

4.3 - Pixel spectrum

The first interesting thing which had to be captured after the selection of the pixel P1 was its reflectance spectrum. The original hyperspectral image caught 195 different bands of the spectrum from about 400 to 2500 nm of wavelength. For this study, the important range was between 400 and 1000 nm. The purpose was to obtain a curve of reflectance to make possible an analytic observation of it. A first solution could be a linear interpolation that it is the simple union of different points to obtain a piecewise line which covers the whole interesting spectrum (however, with a computer software this leads only at another set of points but closer between each other). This solution leads to a rude and difficult to treat function. So, from this fact comes the idea to try to obtain a more treatable function like, for example, a polynomial. To do this, another type of interpolation was done, precisely the least squares interpolation. To find a good compromising between the quality of the final function, conditioning and computational effort in the interesting range of spectrum, a lot of trials were done and the final choice was a 40-degree polynomial.

For the selected pixel P1, Fig. 4.4 shows what explained above, together with ground reference least squares interpolation. The instability at big wavelengths is not important because a mean value can be used to treat some ranges.

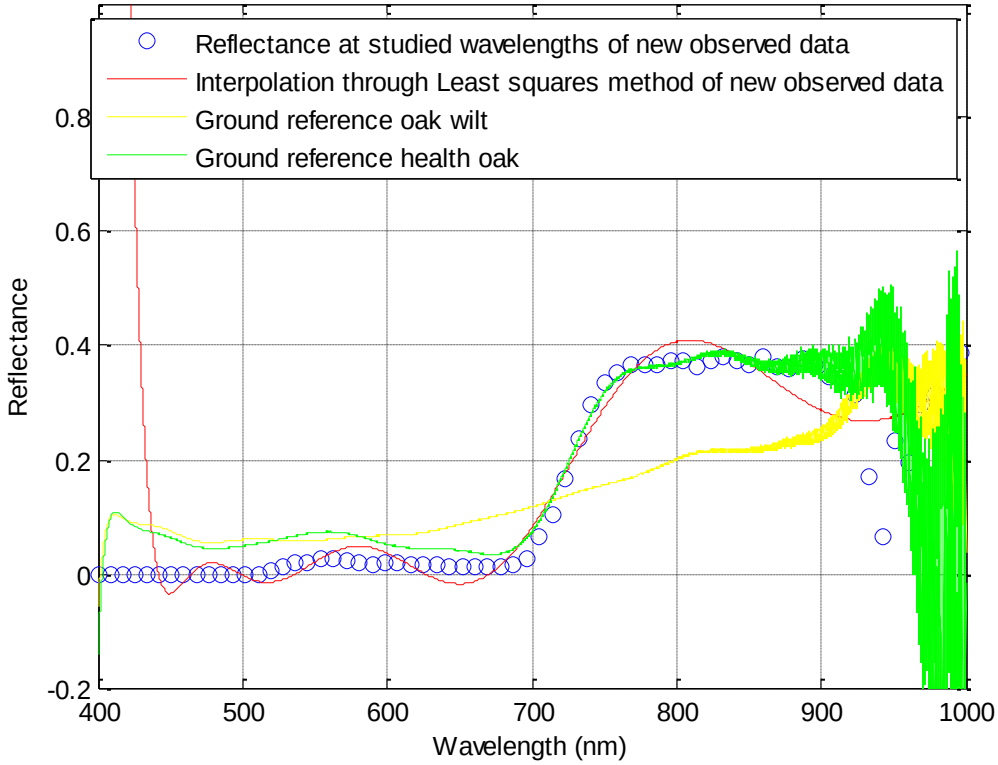

Fig. 4.4. In function of wavelength, reflectance points for new data and reflectance graphs (with least squares approximation), of ground references and new observed data

4.4 - Evaluation of least squares interpolation

Once obtained the least squares polynomial, before continuing it was useful and very important understanding if the function found was a good choice or not. In negative case, the result could be a function too different from the real reflectance spectrum.

A good method for evaluating the accuracy of f is the mean squared error. Precisely, as new observed data there were taken points of linear interpolation and as, estimated ones, points calculated with least squares method. The results (also for ground references), are visible in Fig. 4.5:

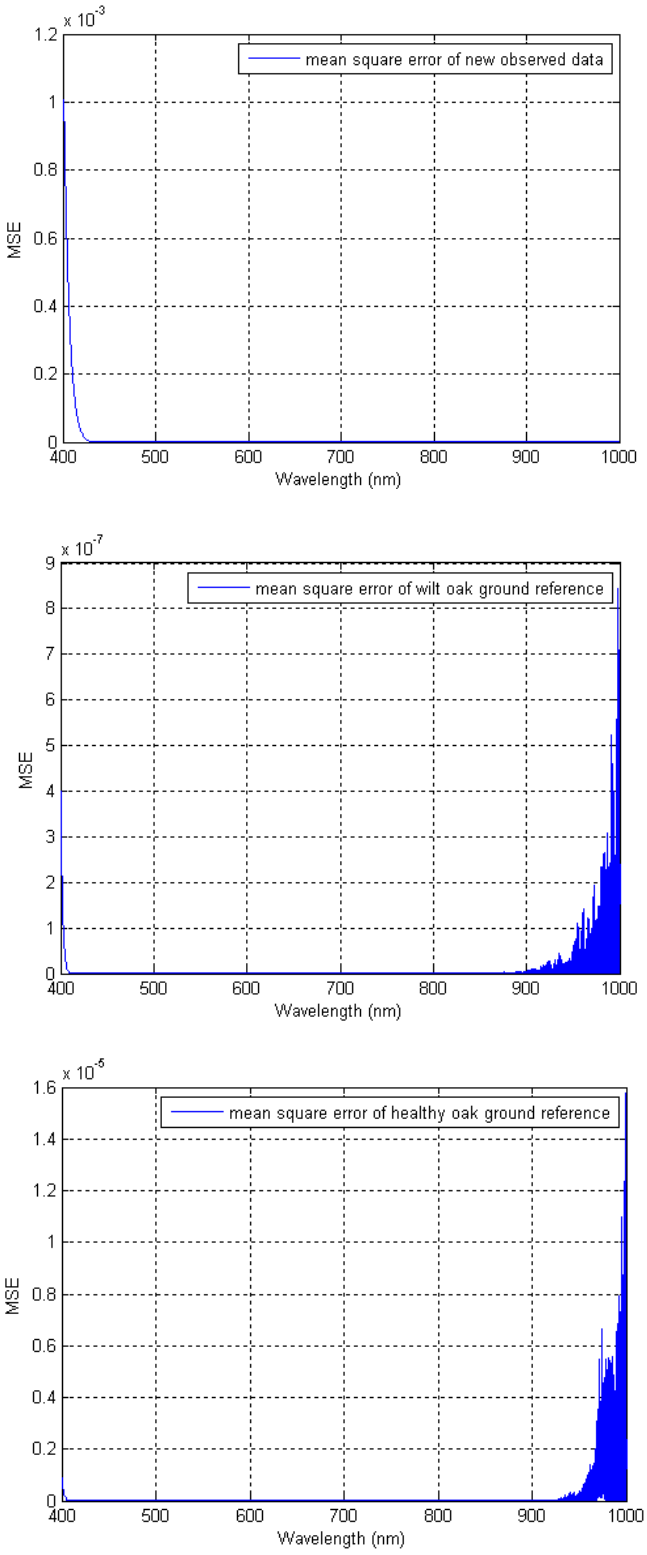

Fig. 4.5. MSE graphs for evaluating least squares approximation

Looking at images is possible noting the very small magnitude of errors in these three curves which indicates that it was taken a good decision regarding the interpolation method. Another observation is that for new observed data, the error is greater than ground reference ones, but this was predictable observing the shape of the curve that is more complicated (however the mean squared error values for each wavelength are good).

4.5 - Derivatives and NWI index

In remote sensing studies from hyperspectral images, it is demonstrated that derivatives are less sensible to variations in illumination intensity but it is also true that signal-to-noise ratio decrease along with the growing of derivative order, so, also in this case, the only opportunity is to find a good compromise (for this work the first 2 derivatives were computed). The final goal here is to prepare good input data for the ANN. Before entering in the study of ANN, some considerations are needed about derivatives. Moreover, it is useful to understand what is the algorithm used for finding them. Starting form least squares approximation of reflectance function, coefficients of first derivative polynomial and (in waterfall), of the second one were found. At this point, the two differential polynomials were evaluated for the same points of initial reflectance function.

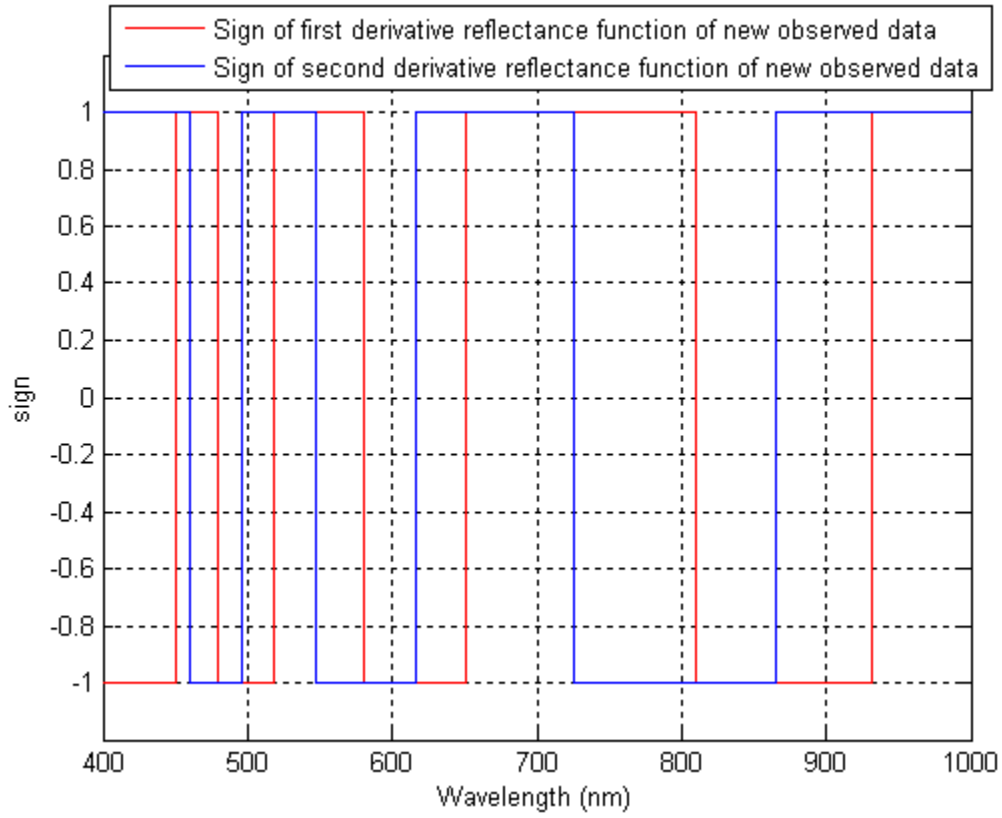

Fig. 4.6. Sign of derivatives for new observed data

Secondly, it was calculated the NWI index and, for the chosen pixel P1 the result was 0.0252; so the expected result from ANN was wilt pixel. In the calculation of NWI, in order to reduce approximation errors, it was used the linear interpolation of reflectance function and the exact formula, thus not the proximate one with derivatives. It is worth saying that this computation were done also for another pixel P (it had NWI = -0.0887), before the one discussed above, in order to train the ANN, as explained in the following paragraphs. For completeness, below (Fig. 4.6), are reported the sign functions of the first two derivatives for P1:

4.6 - ANN

The last remaining steps were the creation of ANN and its evaluation. The target was to discover if an ANN model permits an efficient and precise classification for this kind of problems. Lots of studies were conducted in the past with this technique [4, 8, 10, 11, 12, 13, 14, 15], but quality of results was often low.

The data submitted to the ANN were the following:

Input data:

- Linear interpolation of reflectance function
- Least squares approximation of reflectance function first derivative
- Least squares approximation of reflectance function second derivative

Obviously, it was used one input a time.

Target data:

- Linear interpolation of ground reference of wilt oak trees
- Linear interpolation of ground reference of healthy oak trees
- Least squares approximation of ground reference of wilt oak trees first derivative
- Least squares approximation of ground reference of wilt oak trees second derivative
- Least squares approximation of ground reference of healthy oak trees first derivative
- Least squares approximation of ground reference of healthy oak trees second derivative

The choice of training with healthy ground reference set or the wilt one is guided by NWI value found for pixel P.

These data, during the training of the network were divided into three sets:

- Training set
- Validation set
- Test set

The training method used was the Levenberg-Marquardt backpropagation (Apx. 14), good for regression problems. The training phase created can finish for two main reasons:

- The maximum number of epochs was reached (here 300)
- The performance goal (distance between trained and expected data), was reached, here fixed to 0 (with obvious approximations due to discreteness of computers)

As structure of the network it was used the multilayer perceptron network [5] which has one hidden layer (and one output neuron). After different tests, the best number of neurons (which permits to meet more often as possible performance targets), for hidden layer was discovered (trying from 1 to 12), and precisely was 10. The activation function used was sigmoid tangent. Before starting with classification of images, three different neural networks (one for each degree of derivative calculated), were trained with all combinations of inputs, starting from a selected pixel P. Below (Figs. 4.7, 4.8, 4.9), it is possible to observe different graphs of mean squared errors for an interesting pixel P1 to be classified, using neural networks trained with P.

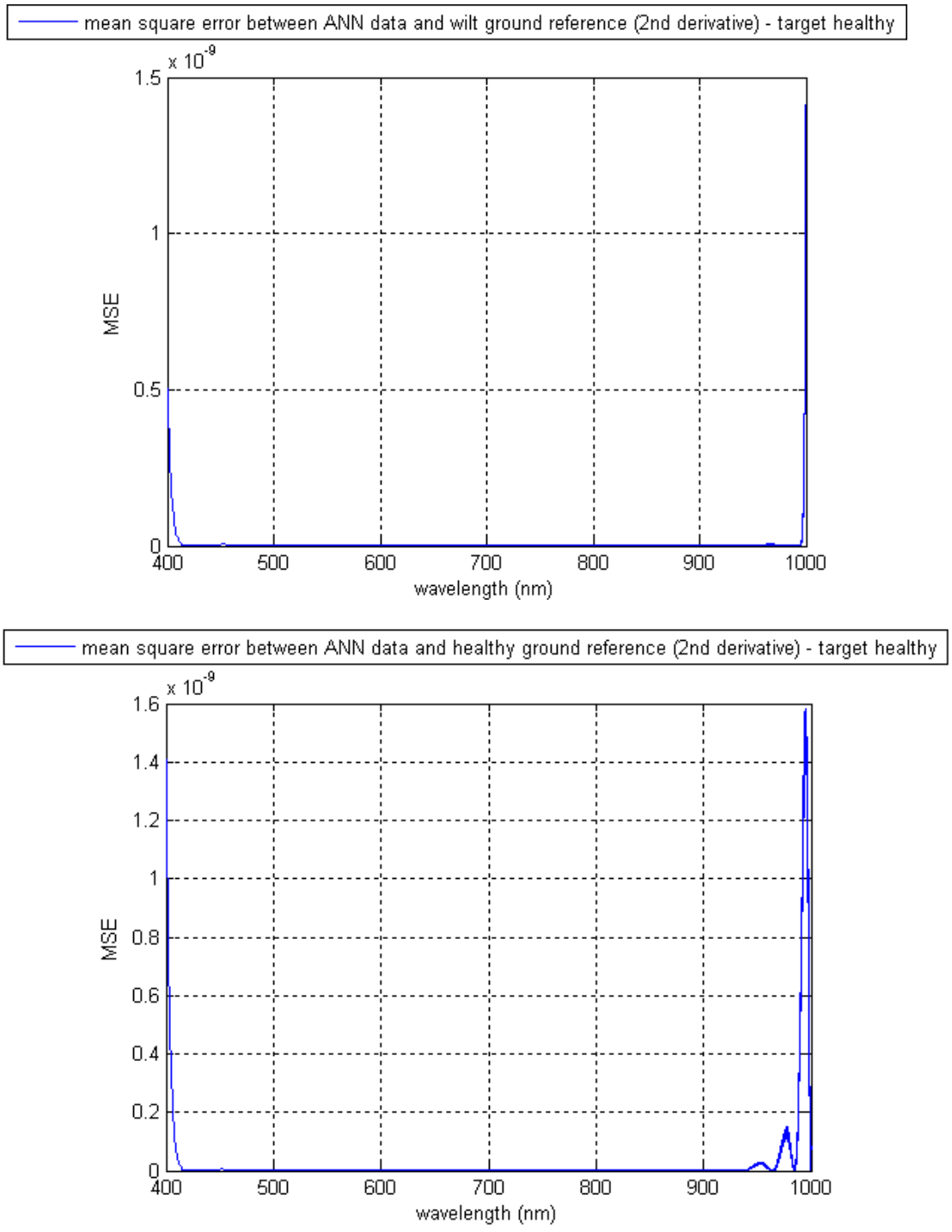

Fig. 4.7. MSE between 2nd derivative of data obtained from ANN and 2nd derivative of ground references, training the net with healthy ground reference

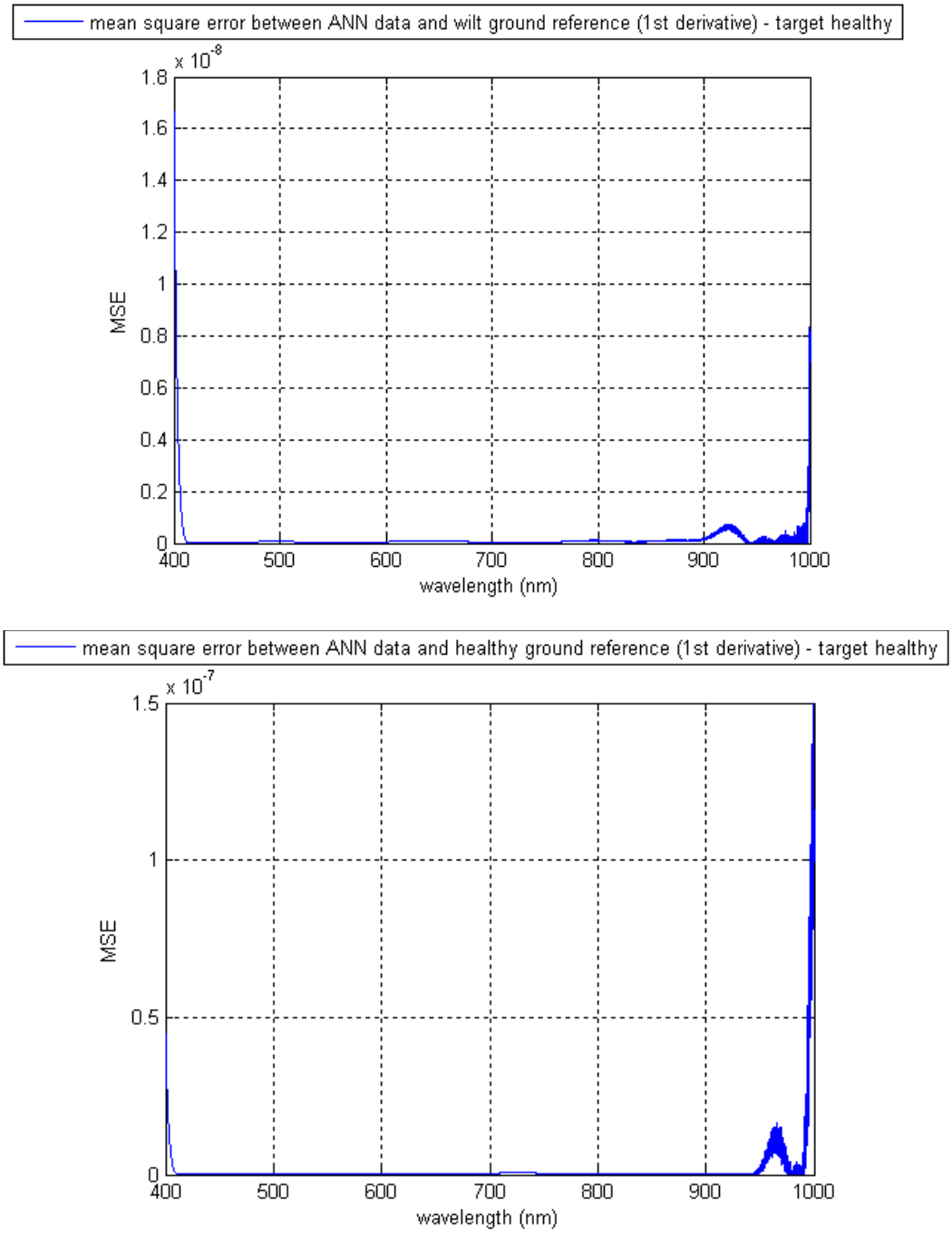

Fig. 4.8. MSE between 1st derivative of data obtained from ANN and 1st derivative of ground references, training the net with healthy ground reference

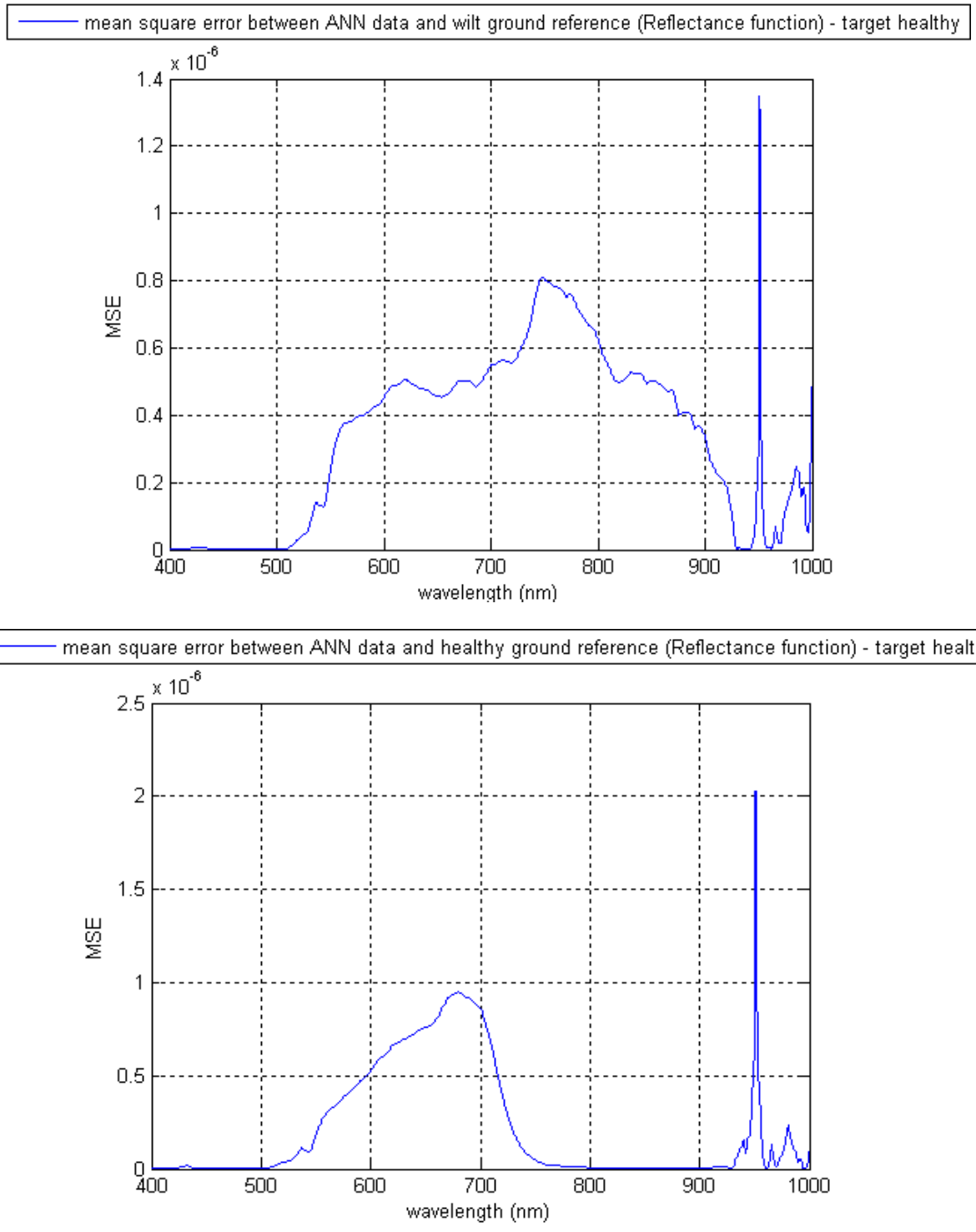

Fig. 4.9. MSE between function of data obtained from ANN and function of ground references, training the net with healthy ground reference

4.7 - Comment on results

After observing these pictures, it is important to understand how to interpret them.

For pixel P, the NWI was negative, so the three ANNs were trained with healthy ground reference. The three results for pixel P1 (with NWI positive), were compared with respective ground reference derivative degrees (both wilt and healthy ones) to obtain Fig. 4.7, 4.8, 4.9. Looking at the graphs it is possible to observe that (mostly for reflectance function, for the others differences are too small to be significant), looking at the red band (for example between 600 and 700 nm), mean MSE for wilt ground reference is slightly minor, so for P1 is confirmed the NWI found.

Other tests confirmed what written above, but an observation in useful: often, results regarding first and second derivatives were not reliable (this was discovered looking at many MSE graphs). This problem was due to the fact that ANNs are ineffective for this kinds of problems; although the least squares method was precise, it was not enough for having a stability of output behavior. To improve this situation, one possible solution was to try another interpolation method, such as a spline one. Because of the suitability of derivatives for these kinds of problems it was crucial to find a solution.

Another important thing to say is that results of classifications are subject to the training of neural networks, so, if necessary, it is wise doing more trials for having nets trained with accuracy (this means that different training pixels can be used and evaluated each time).

5 – A Refinement of ANNs study

Below are proposed refinements and reached results about what it is discussed in the previous Chapter.

5.1 Introduction

As seen in the previous chapter, it is difficult working with good approximate data. The least squares method does not permit to force the approximation line to pass through known point of the spectrum, so the result is often not reliable. Moreover, also when it is correct, the boundary between right and wrong evaluation is very slight and this bring a lot of doubts about the quality of the method because there is not a safety diagnosis. What is exposed in the present chapter is the same study but with different interpolation method, the cubic spline one. Ground references and hyperspectral images used are the same of the previous Chapter. Moreover, attempts to improve the quality of the study by changing the transfer function are presented.

5.2 – Spline - The proceedings

Once obtained ground references, using cubic spline method, first and second derivatives were calculated. NWI index was computed exactly as in Chapter 3. To evaluate the quality of the interpolation it is useful to observe the following image (Fig. 5.1), in which is possible to see that the difference between linear and cubic spline interpolation is really minimal.

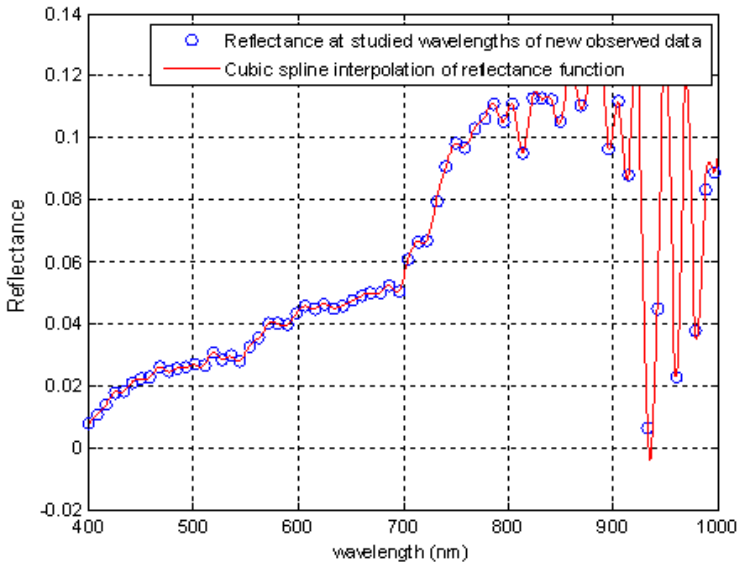

Fig. 5.1. In function of wavelength, examples of reflectance points for new data and reflectance graph (with cubic spline interpolation), of new observed data

A quick comparison with Fig. 4.4 clearly shows that this interpolation is better. In order to obtain derivatives it was followed a procedure similar to the previous, but with the spline method a set of polynomials is considered (one for each sub-interval), so that the degree of each one is low and conditioning problems are overcome.

Regarding the ANN, it was used the same architecture of Chapter 1. In Figs. 5.2, 5.3, 5.4 are reported MSE graphs with the same meaning of Figs. 4.7, 4.8, 4.9 but different interpolation.

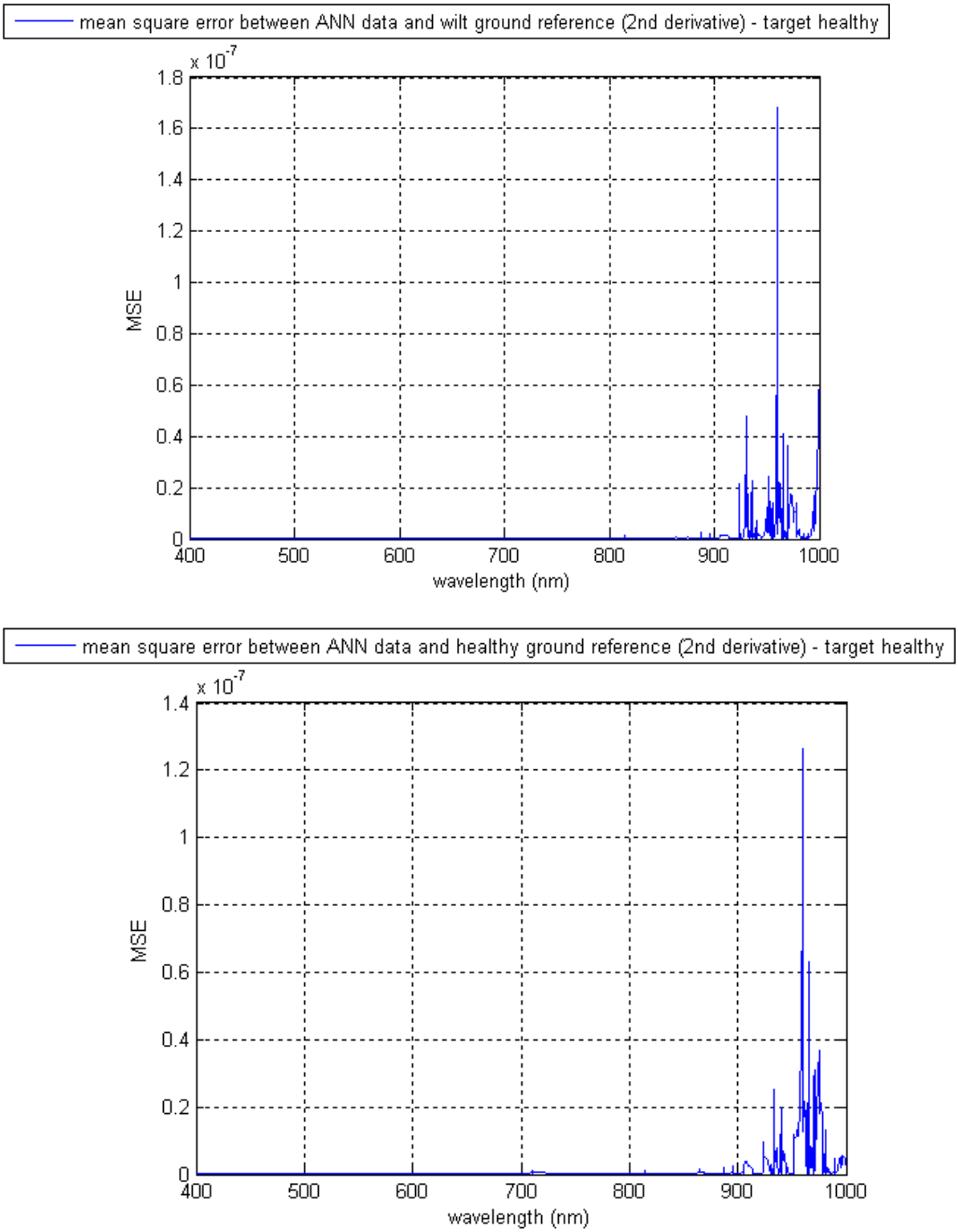

Fig. 5.2. MSE (for data interpolated with spline), between 2nd derivative of points obtained from ANN and 2nd derivative of ground references, training the net with healthy ground reference

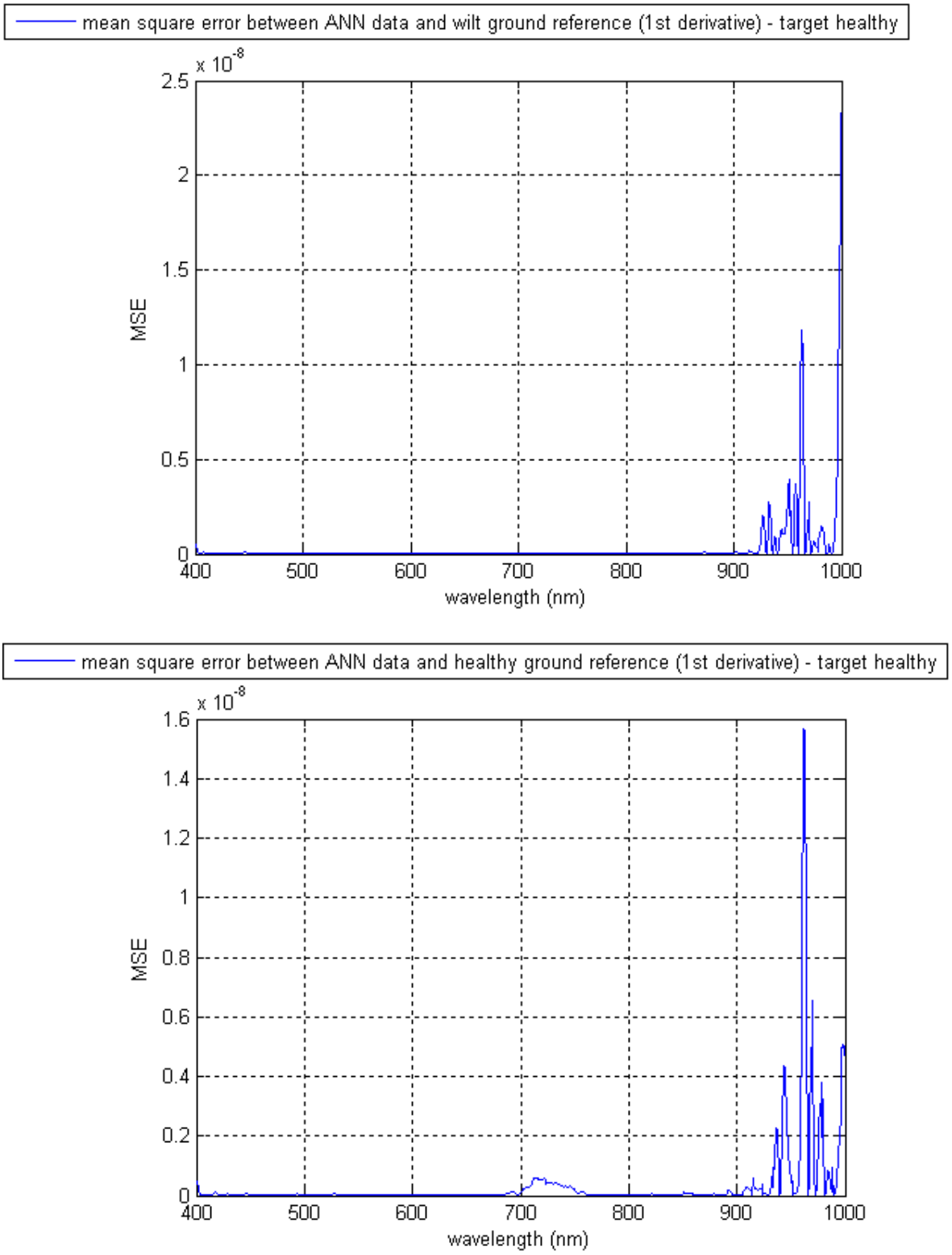

Fig. 5.3. MSE (for data interpolated with spline), between 1st derivative of points obtained from ANN and 1st derivative of ground references, training the net with healthy ground reference

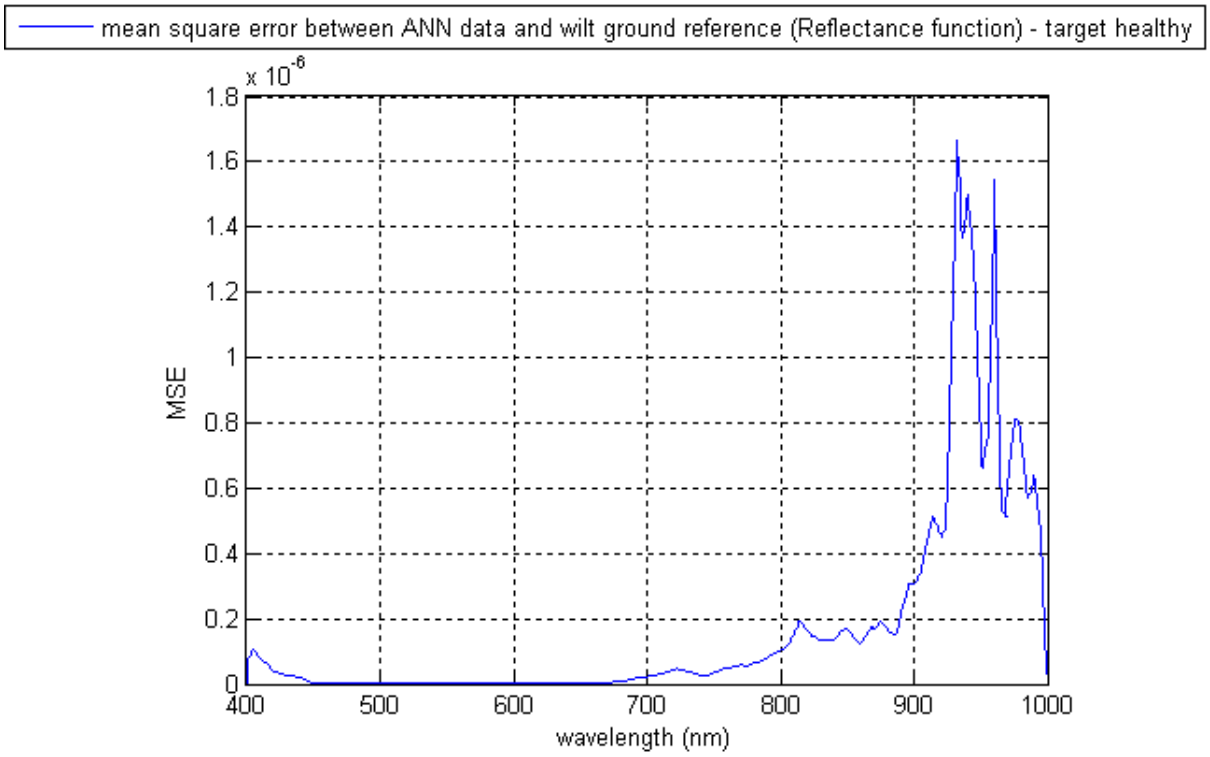

Fig. 5.4. MSE (for data interpolated with spline), between reflectance function of points obtained from ANN and reflectance function of ground references, training the net with healthy ground reference

5.3 – Considerations about Spline

As it can be seen from Figs. 5.2, 5.3, 5.4, where starting from an ANN trained with a pixel P having NWI = -0.034 and trying to classify a pixel P1with NWI = 0.056, even in this case there are no strong differences between graphs of each pairs. However, function and derivatives are indeed more accurate than in chapter one, so it is reasonable going into detail more than what was done before and it was convenient to see mean values in red band of wavelengths (that in general is more significant than others for vegetals). Fig. 5.5 shows values.

	Reflectance	**Reflectance's 1st derivative**	**Reflectance's 2nd derivative**
Healthy	0.0387	2.2609 e^{-7}	3.3573 e^{-11}
Wilt	0.0384	6.4604 e^{-7}	6.6693 e^{-11}

Fig. 5.5. Mean values of red band for graph in Figs. 5.2, 5.3 and 5.4

Looking at these values it is possible to note that only using reflectance function there is a good result (MSE minor for wilt oak pixel, as expected, but with a very small difference). This leads to conclude that, also with this improvement, ANNs are not good enough for a problem like this one. Other tests for the same models confirmed this assumption. Moreover, also in the present case, the most accurate function is the original reflectance one, so the derivatives are also here not enough reliable.

5.4 – Attempts with other transfer functions

In all previous tests, as activate function it was always used sigmoid tangent. Here it is proposed a study using as transfer function sigmoidal logarithm, the best among tested functions. The networks were trained starting from a healthy pixel (NWI= - 0.0101). Following the same process as before, with cubic spline, it was possible to obtain the following graphs, Figs. 5.6, 5.7, 5.8.

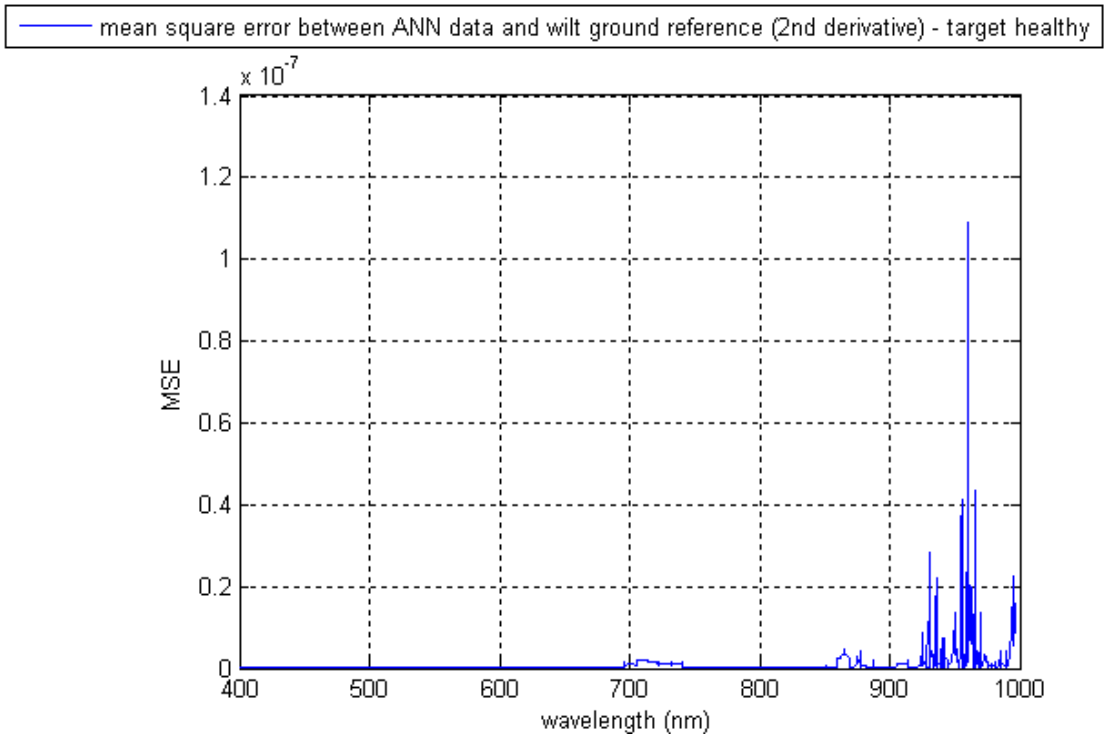

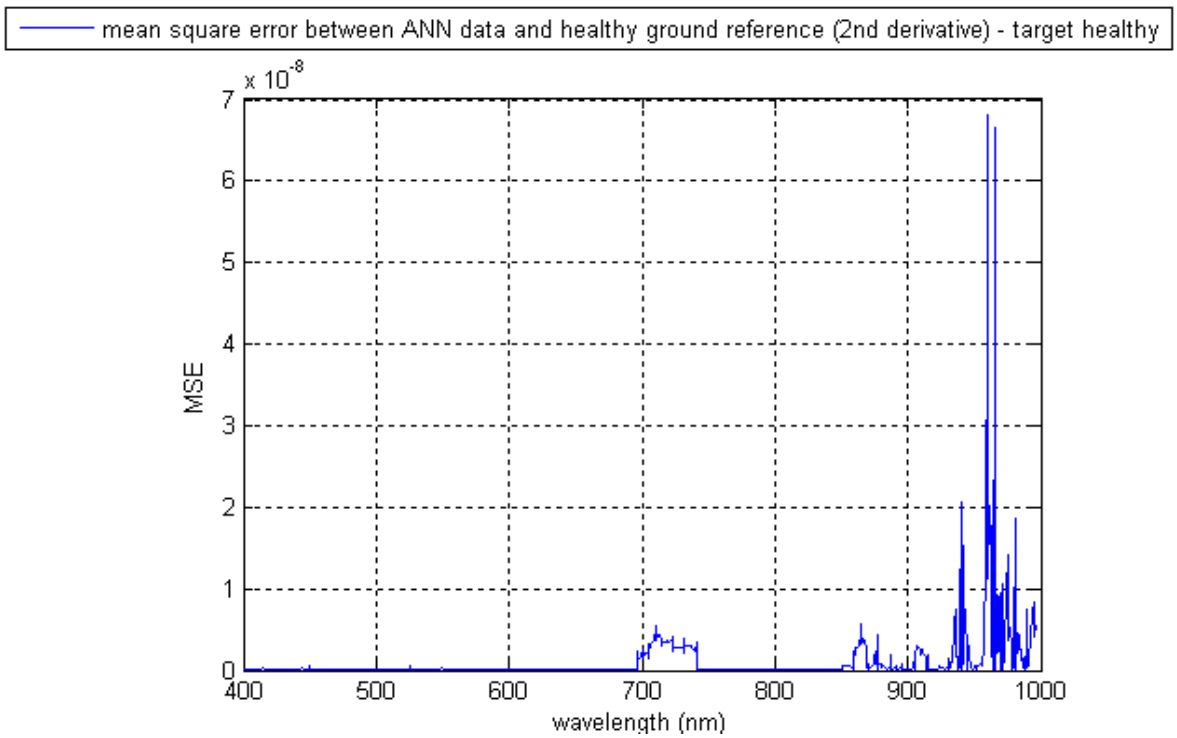

Fig. 5.6. MSE (for data interpolated with spline), between 2nd derivative of points obtained from ANN and 2nd derivative of ground references, sigmoidal logarithm as transfer function and training the net with healthy ground reference

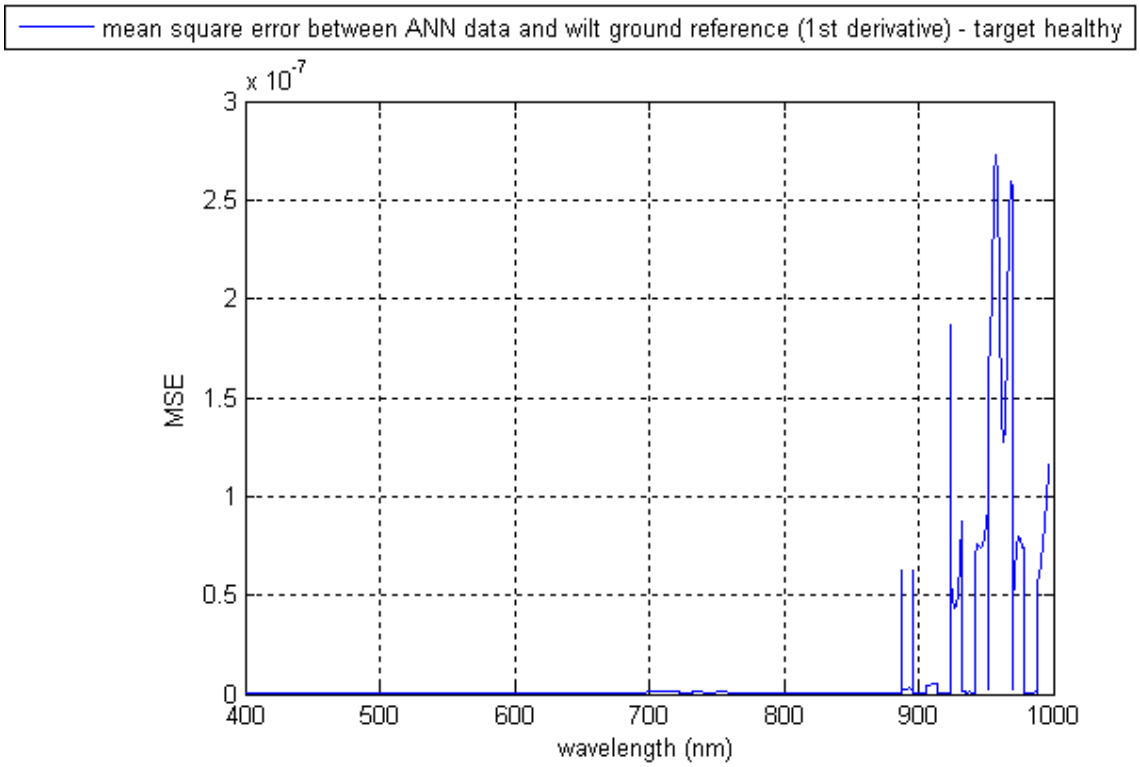

Fig. 5.7. MSE (for data interpolated with spline), between 1st derivative of points obtained from ANN and 1st derivative of ground references, sigmoidal logarithm as transfer function and training the net with healthy ground reference

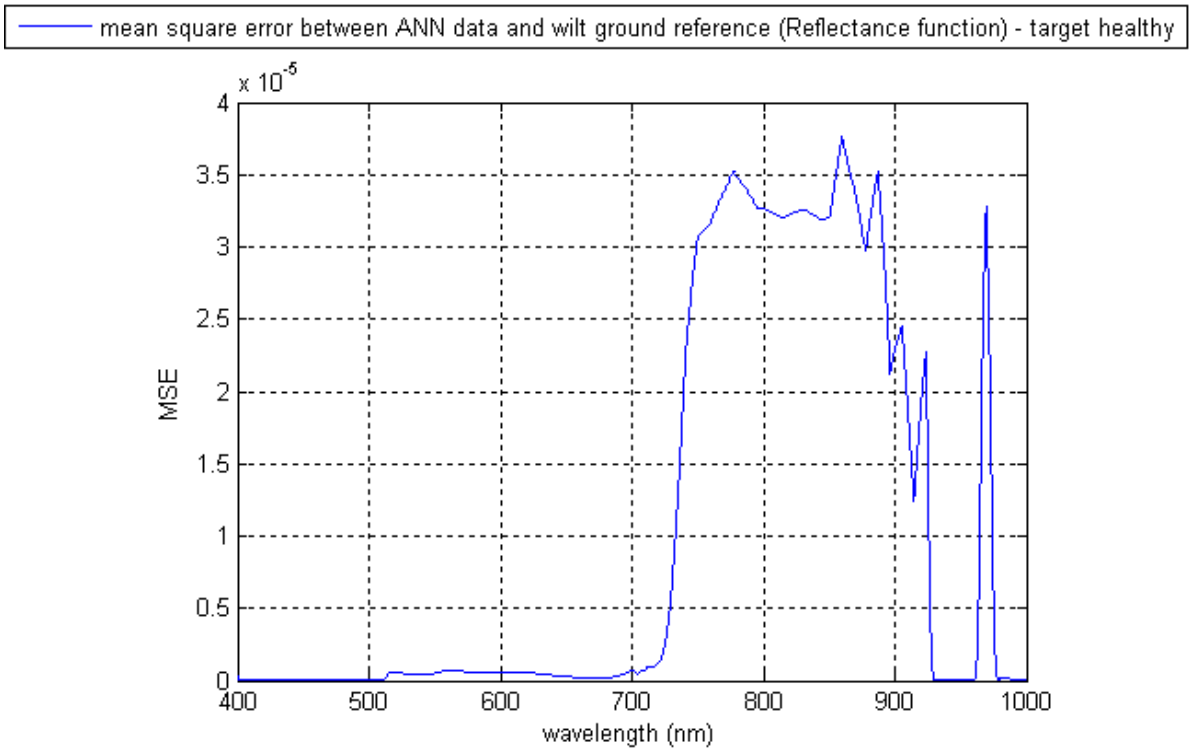

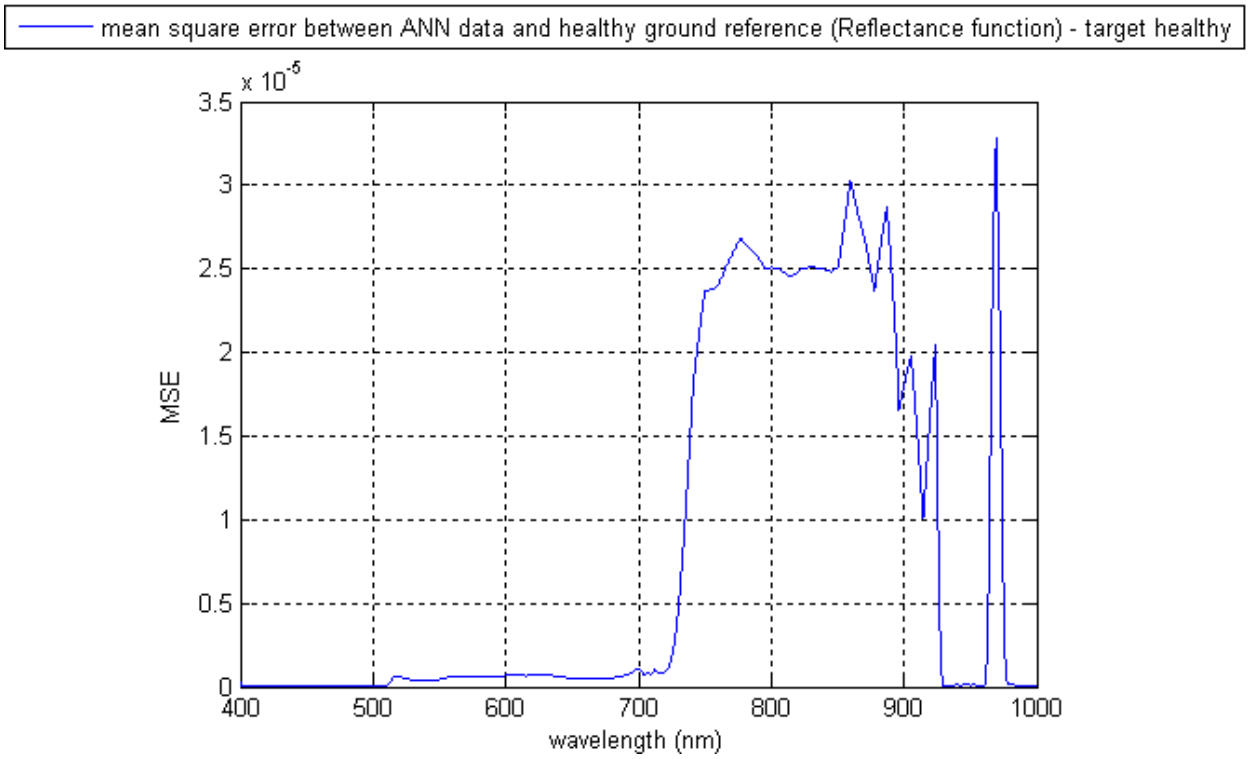

Fig. 5.8. MSE (for data interpolated with spline), between reflectance function of points obtained from ANN and reflectance function of ground references, sigmoidal logarithm as transfer function and training the net with healthy ground reference

In this particular case the test was done for a healthy pixel, with estimated NWI= - 0.1048.

Mean values in red band are reported below (Fig. 5.9):

	Reflectance	**Reflectance's 1st derivative**	**Reflectance's 2nd derivative**
Healthy	0.0508	6.2587 e^{-7}	1.7881 e^{-11}
Wilt	0.0505	4.8465 e^{-7}	6.1693 e^{-11}

Fig. 5.9. Mean values of red band for graph in Figs. 5.6, 5.7 and 5.8

Even in this case it is useful a more precise comment about. Differently from other cases, here (and also for other treated cases), the most accurate value as expected regards 2nd derivatives, so, this is a good result. But the problem is due to the fact that differences are too small, and for 1st derivative and reflectance function the result is wrong, so it was impossible working with this model with a good degree of certainty. As other attempt of improving ANN approach, it was used a linear transfer function but with bad results; in fact, mean values were always better for wilt pixels. Also trying to consider other ranges of reflectance spectrum instead of red one, the outcome did not improve.

To summarize the results shown in these Chapters (4 and 5), NWI performs better than ANNs for a study like this, in the sense that results are more reliable and easily understandable. Since the achieved results are not satisfactory, a different approach has been considered. Next Chapter describes an approach based on the shape of reflectance graphs (instead of using reflectance coefficients). As we will see, it performs extremely good.

6 – Static GTI

Because of inefficiency of ANNs approach a new procedure had to be developed. Here it is presented a rule-based mechanism to automatically classify pixels looking at a fixed threshold.

6.1 - Introduction

GTI (Growth Threshold Infra-Red) method represents a different approach to study phenomena like the one discussed in this work. It was chosen to follow a strategy rule-based as presented below. In particular, this method is focused on the observation of reflectance graphs and permits to create a very accurate map of the diffusion of some characteristics (like an epidemic), in a zone [26]. To work in properly way it requests a lot of observations in order to get higher accuracy, as explained in the following paragraphs. The study deals with oak trees, but at the end of the chapter how to use GTI investigation also for other kind of plants is discussed.

6.2 - Reflectance graphs – A different way to observe them

To conduct a study using reflectance graphs, two ingredients are required: ground references and new observation-reflectance graphs. It is useful to propose here again (Fig. 6.1), the ground reference shapes for one pixel of a hyperspectral image:

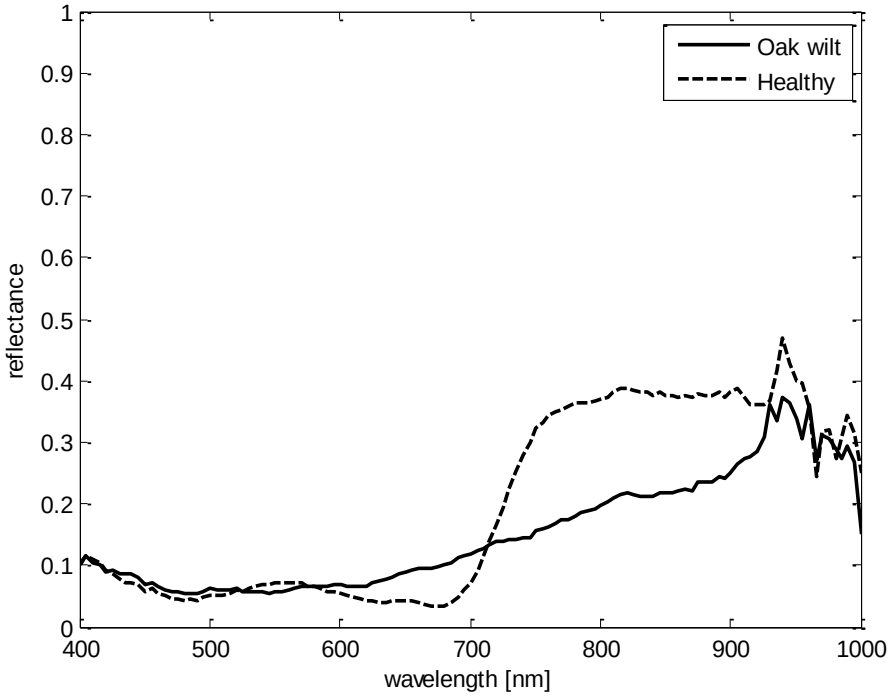

Fig. 6.1. Reflectance graphs for ground references, in function of wavelength

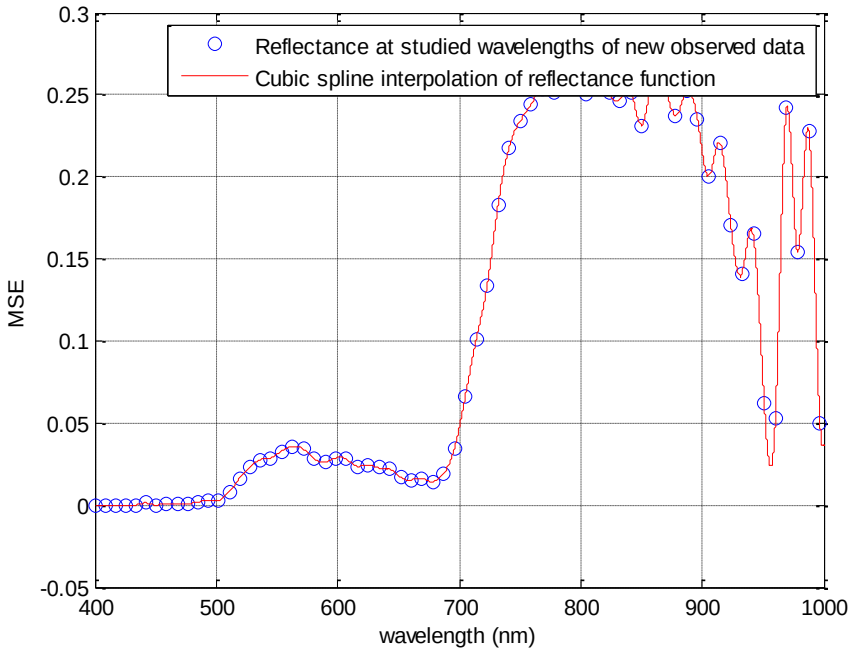

Fig. 6.2. Reflectance graphs for a new observed pixel, in function of wavelength

Looking at previous graph it is possible to observe one really interesting thing: during the wavelength range [27] 700-750 nm (the initial part of Near Infra-Red), healthy oak have a huge increment of their reflectance while wilt trees not.

Instead, Fig. 6.2 shows reflectance graph for a new observed pixel:

The NWI index is -0.2276 and observing the shape of Fig. 6.2, it is possible to note that is very similar (mostly in 680-750 range), to the healthy ground reference. Value of reflectance are very different, in fact it is possible to observe that in Fig. 3.1 in the range mentioned before, growing is from about 0.1 to 0.35; instead, in Fig. 3.2 about from 0.05 and 0.25. But one characteristic is actually important: the percentage growth respect to the total one. In the first case is 83.3% and in the second 76.9%. The following image (Fig. 6.3), shows a graphical representation of these percentages:

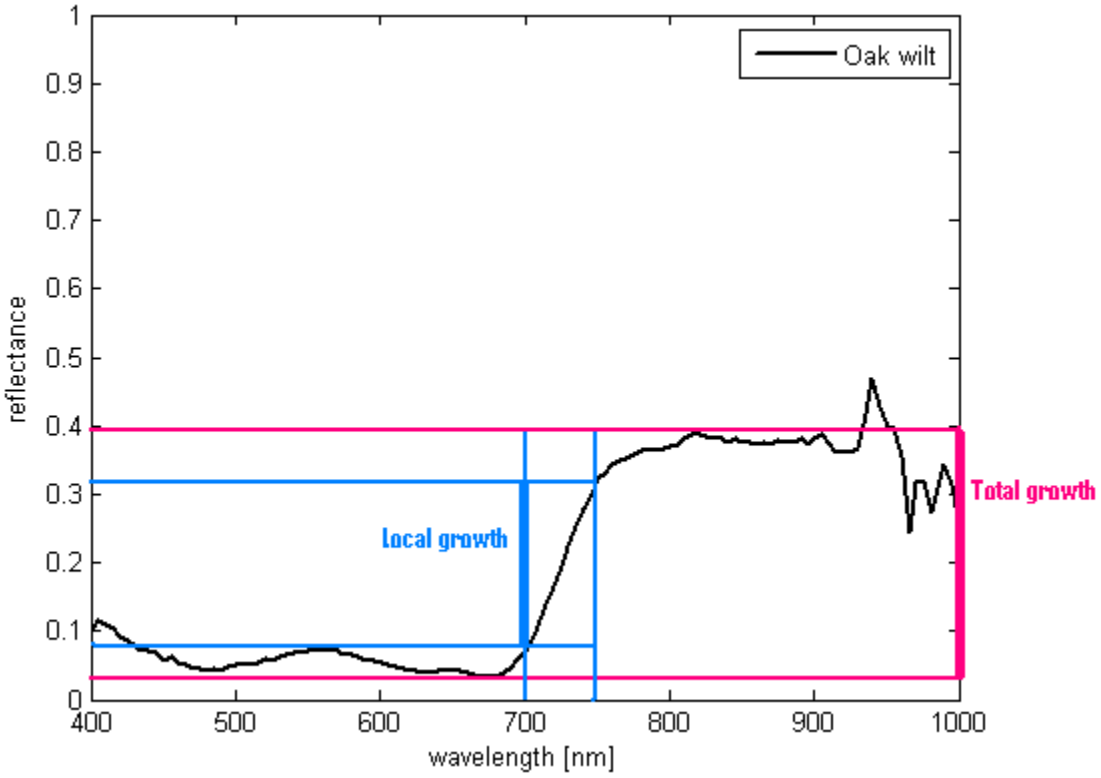

Fig. 6.3.. A graphical interpretation of the percentage study about reflectance growth

Observing a lot of reflectance shapes, it was possible to observe that it could be reasonable looking for a threshold (equal for each image representing oak trees, for this reason the method could be called Static GTI), of the percentage local growth to sign a boundary between wilt and healthy oaks. Experimental results lead to these rules:

$$local\ growth \geq 0.6 \times total\ growth \Rightarrow healthy\ oak\ trees \quad (12)$$

$$local\ growth < 0.6 \times total\ growth \Rightarrow wilt\ oak\ trees \quad (13)$$

Where:

Def. 6.1. $local\ growth$ is the difference between values of reflectance spectrum in 680 and 750 nm.

Def 6.2. $total\ growth$ is the difference between maximum and minimum peaks of reflectance spectrum in the range 400-900 nm.

6.3 – About autumn

The color of autumnal leaves [28] can represent a problem, mainly using eye observations. Moreover, the reflectance spectrum (Fig. 6.4), has a different shape from the ones considered before:

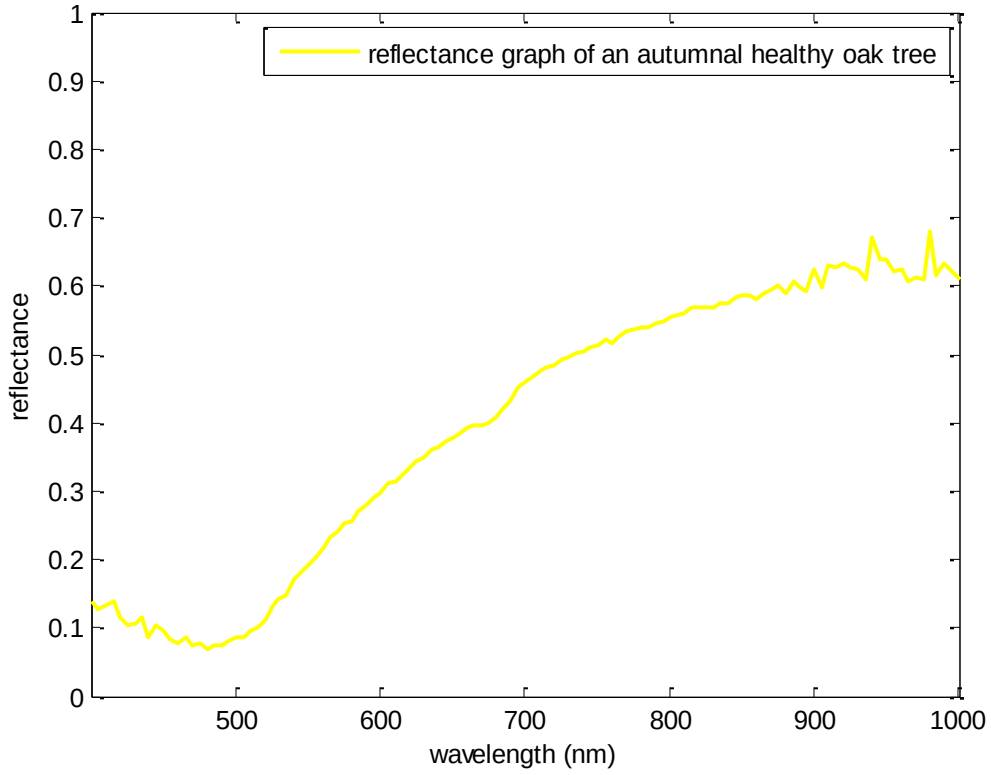

Fig. 6.4. Reflectance spectrum for autumnal healthy oak tree

But even in this case, percentage growth was useful. Looking at the range between 500-600 nm of Fig. 6.4, it is possible to note a phase of large increment of reflectance values (this was then confirmed by observing a lot of graphs). Moreover, it was observed that for autumnal pixels, between 600 and 680 nm there was a downwards concavity (observable through a study based on the second derivative). So, noting that these feature can discriminate between autumnal and not autumnal plants, it was possible to define a refinement about autumn:

$$((autumnal\ growth\ \geq\ 0.15 \times total\ growth)\ \&\&\ (autumnal\ concavity \geq 0)) \Rightarrow\ healthy\ autumnal\ oak\ trees \quad (14)$$

$$else$$

$$(local\ growth < 0.6 \times total\ growth)\ \Rightarrow\ wilt\ oak\ trees \quad (15)$$

Where:

Def. 6.3. *autumnal growth* is the difference between values of reflectance spectrum in 600 and 500 nm.

0.15 is the autumnal threshold

Def. 6.4. *autumnal concavity* is the average of second derivative coefficients in the range between 600 and 680 nm.

So, (14) is better than (12).

6.4 – Application of the method

Starting from Fig. 4.2 which is optimized, it was conducted a study regarding one of its regions. So, once selected a rectangular area, (12), (14) and (15) were applied for each pixel in order to evaluate the illness.

The result is showed in Figs. 6.5a and 6.5b:

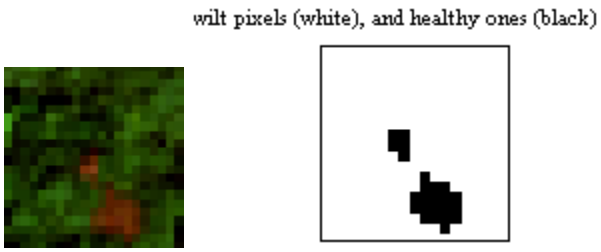

Fig. 6.5. (a) The selected area; (b) The result

It is important to say that this method permits a good identification also in zones in which is not possible to distinguish ill pixels with only eye observation.

6.5 – Attempt with not optimized images

Looking at previous paragraphs, it was clear the robustness of the GTI method for optimized images. Here it is proposed an example of GTI application for a not-optimized image captured during June 2009 (Figs. 6.6, 6.7a and 6.7b):

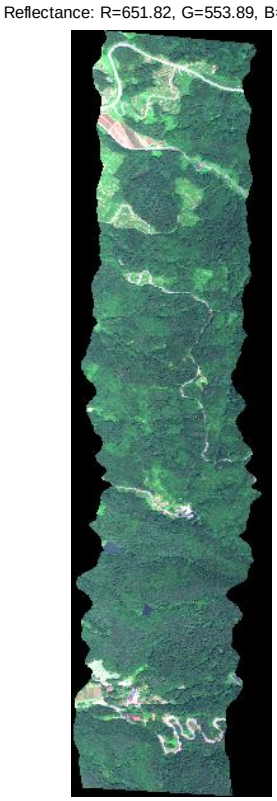

Fig. 6.6. Not-optimized image studied

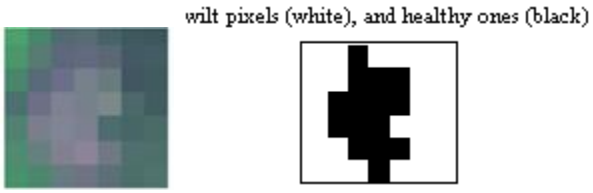

Fig. 6.7. (a) The selected area; (b) The result

From images above it is possible to note a good result, so GTI method can be used also for not-optimized images (for images of August 2009 the result was optimal too). But in general the outcome was more accurate for modified images, as expected. Nevertheless this method can be a good starting point for the study, able to intercept ill zones with a good but not optimal precision. To get a more detailed response it is possible to do modifications to the image and then repeat the procedure.

6.6 – Considerations

This kind of work requests for each pixel the reflectance graphs and this represents a big computational effort. So, in absence of an adequate computing power a better way to act is to select small areas. For example, analyzing 500 pixels with a PC equipped with Pentium 4 ® 3.80 GHz, 1 GB of RAM which takes images from a server using a LAN connection, takes about 4 minutes. But GTI takes however much less time than ANN to do the same work and its even much better. About the threshold, to identify the best one, the only real good way to work is observing more pixels as possible and finding a good value. In this case, 0.6 could be improved, but the value found is already good.

6.7 – A general vision of GTI

This method, applied to oak trees, gives excellent results[1]. Now, one question comes natural: is it possible to extend GTI also to other vegetal species? Considering other species, it was seen that also for rice fields and grass fields, it was possible to find a threshold for discriminating between wilt and healthy pixels (with a different disease respect to previously analyzed oaks and this is crucial), so, in conclusion, it is reasonable saying that such approach can be generalized to understand the illness of different species. In general a good way to act is to observe reflectance graphs for a lot of pixels, understanding what could be the threshold and then evaluationg the model found with the help of ground references in order to compare results and understanding the quality of the work.

So, in general, GTI method for specie i can be explained as:

$$((autumnal\ growth\ \geq\ \theta_{ai} \times total\ growth)\ \&\&\ (autumnal\ concavity \geq 0)) \Rightarrow\ healthy\ autumnal\ oak\ trees \quad (16)$$

$$else$$

$$(local\ growth < \theta_i\ \times total\ growth)\ \Rightarrow\ wilt\ oak\ trees \quad (17)$$

Where θ_i is the threshold of specie i and θ_{ai} .is the autumnal one.

[1] for optimized and not – optimized images in good environmental conditions. Low quality images are considered in the next chapter

6.8 – Other examples

The following images (Figs. 6.8, 6.9, 6.10, 6.11, 6.12 and 6.13), show examples of application of GTI method in different sets of images for oak trees (reflectance - optimized and not).

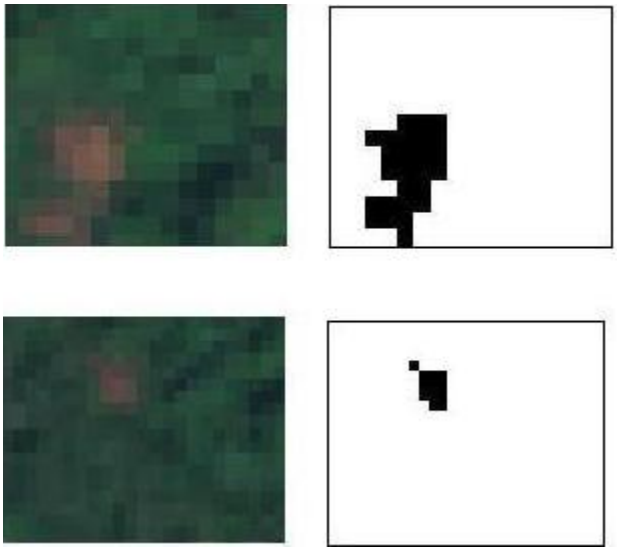

Fig. 6.8. Regions of a not-optimized reflectance image captured during June 2009

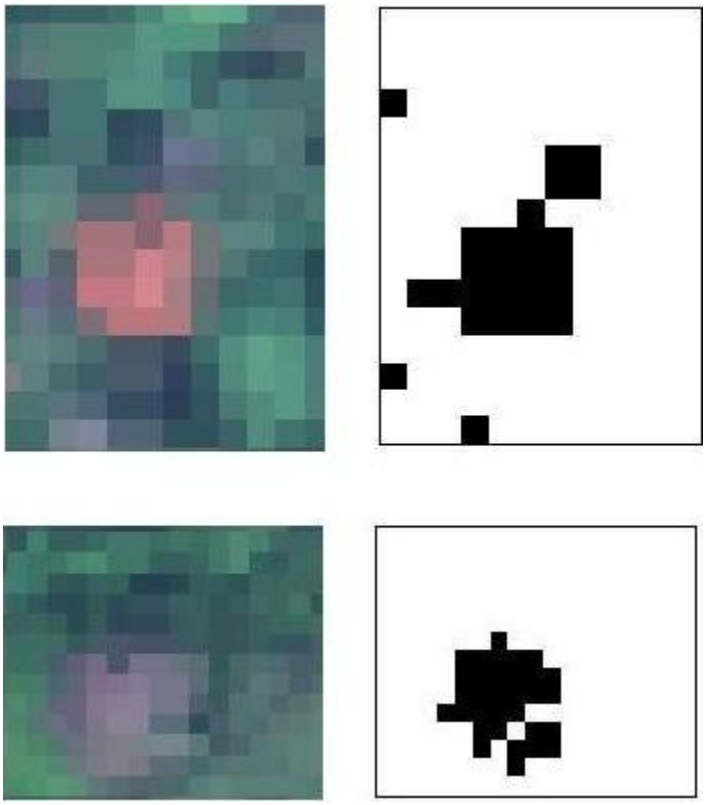

Fig. 6.9. Regions of another not-optimized reflectance image captured during June 2009

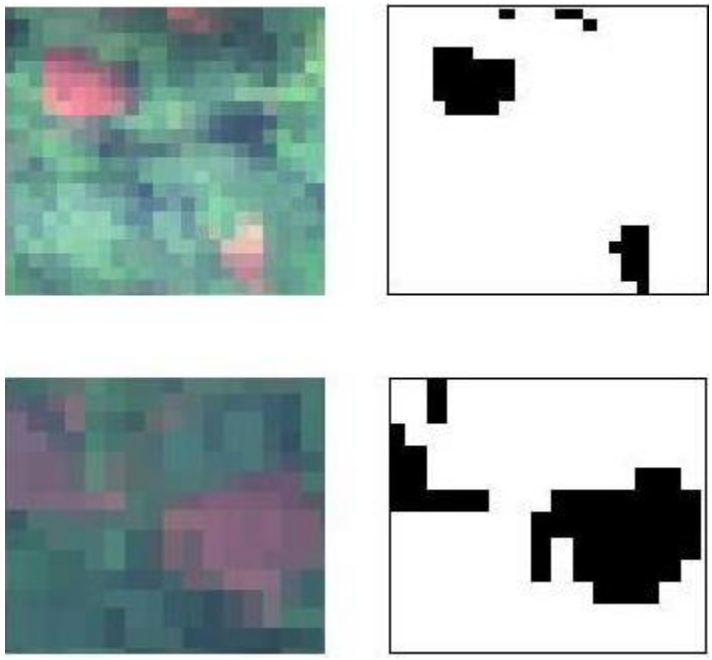

Fig. 6.10. Regions of a not-optimized reflectance image captured during August 2009

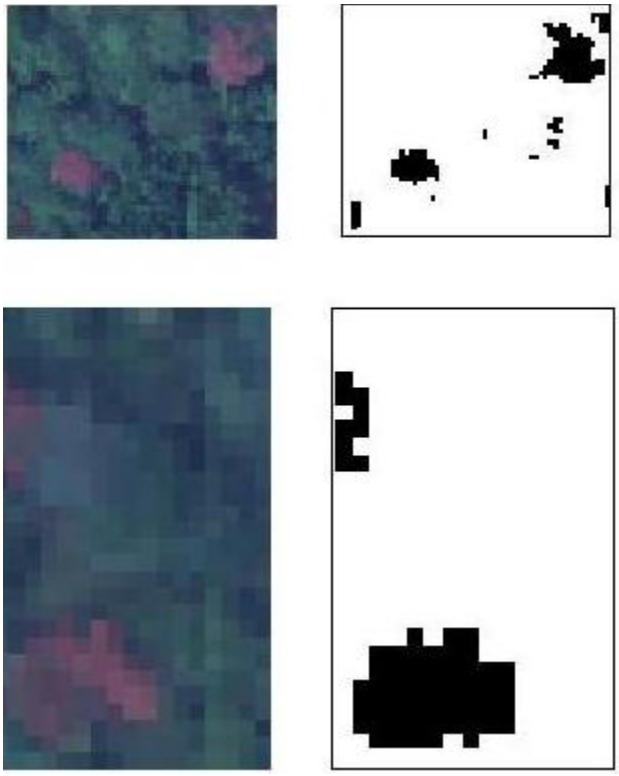

Fig. 6.11. Regions of another not-optimized reflectance image captured during August 2009

22 ottobre 2010

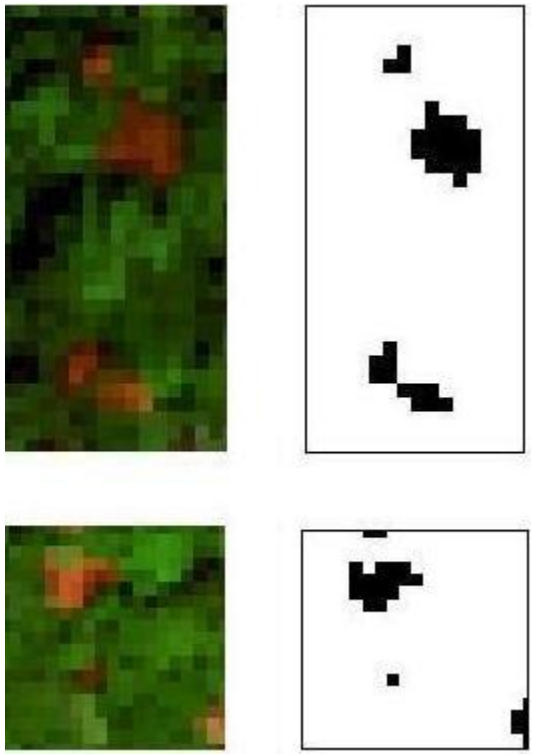

Fig. 6.12. Regions of an optimized reflectance image captured during August 2008

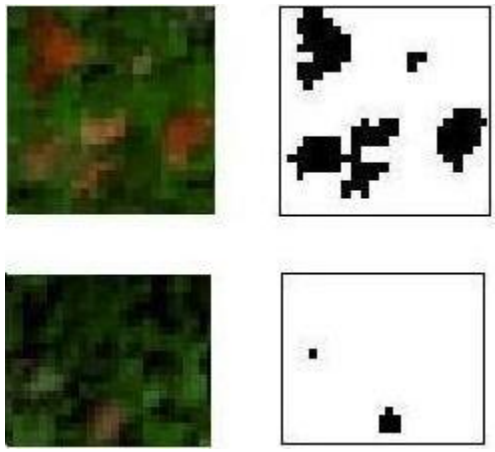

Fig. 6.13. Regions of another optimized reflectance image captured during August 2008

6.9 – Application of GTI for rice fields

Below it is proposed an example of a studying regarding rice fields (Fig. 6.14), in order to demonstrate the good functioning of GTI also for this type of vegetal.

Fig. 6.14. A Japanese rice field

In particular there were used not-optimized reflectance images and this way of acting is excellent to test the quality of the model because, in general, if GTI works well for not-optimized images, it will work better for modified ones. Obviously, there were used other images, captured with the same method of the others explained during all the present treatment, in particular, not-optimized images of August 2008 regarding Japanese rice fields affected by Rice blast (precisely in Syonai Suito district), that it is a different disease with respect to the one of oak trees (Apx. 8). In Fig. 6.15 is possible to observe an example:

Fig. 6.15. Not-optimized reflectance image of rice fields

As usual, starting from Fig. 6.15 it is possible to select a region and then zooming it (Fig. 6.16a):

Imposing, after a lot of attempts, a threshold θ of 0.6, it was been possible to obtain the following image (Fig. 6.16b):

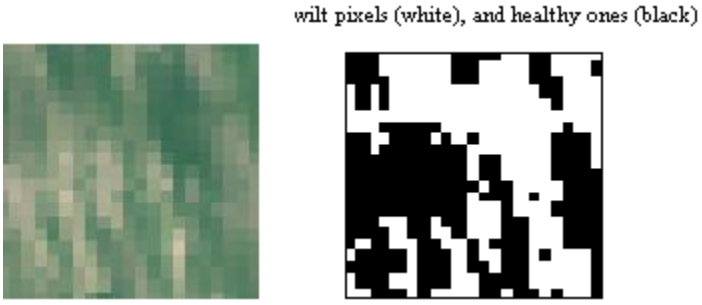

Fig. 6.16. (a) Region of Fig. 6.17; (b) Final GTI result about Fig. 6.17

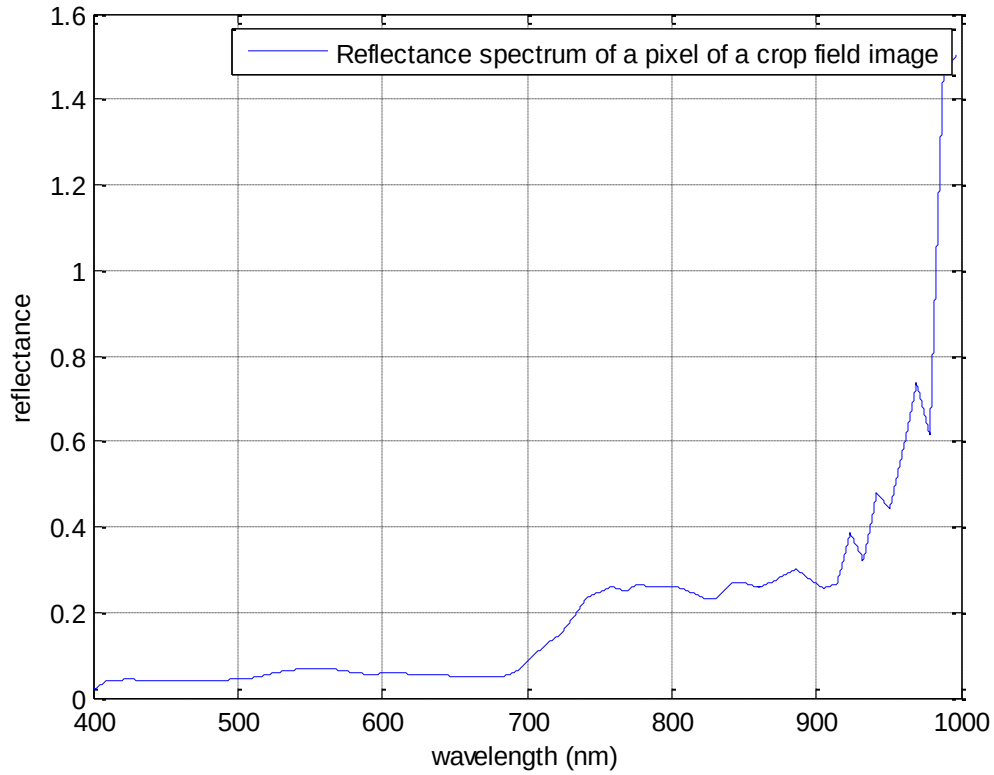

Fig. 6.17. Reflectance spectrum (not – optimized), for one pixel

In Fig. 6.17 there is a reflectance spectrum about one observed pixel.

Looking at this image, it is simple to observe that, in range spectrum 400 – 900 nm, the maximum growth interval is also in this case 700 - 750 nm as desired. So, this is another confirmation which it is possible to perform a study similar to the one regarding oak trees.

6.10 – Application of GTI for grass fields

As other example about GTI there were considered also different types of Japanese grass species (in Fig. 6.18 is possible to view an example).

Fig. 6.18. A Japanese grass field

Starting from airborne images captured during 2008 (there is an example in Fig 6.19), it was evaluated the possibility of using with success the method. Just only with an observation of proposed graph (Fig. 6.20), it is possible noting that the range 700 - 750 nm is even in this case very important because it includes the biggest growth of reflectance (reflectance was not optimized). Moreover, this study explained another interesting thing: GTI can permits also classification of different species of grass, so it can be used not only for diseases detection.

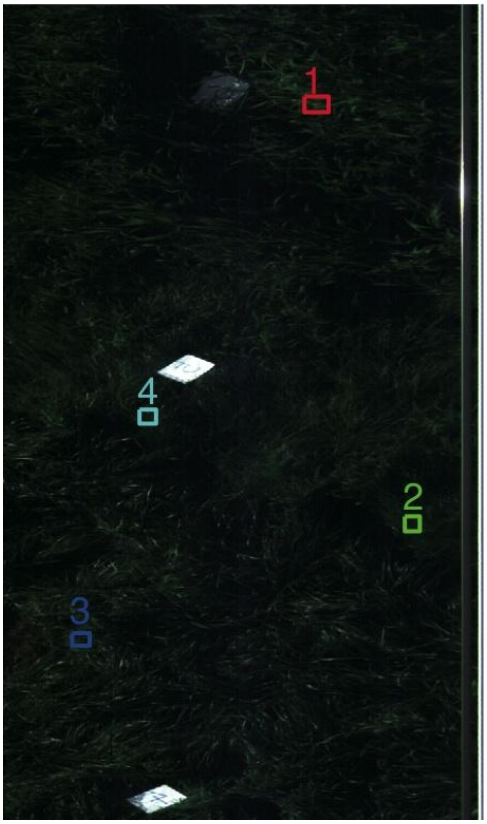

Fig. 6.19. Airborne image of grass field with observed pixels marked

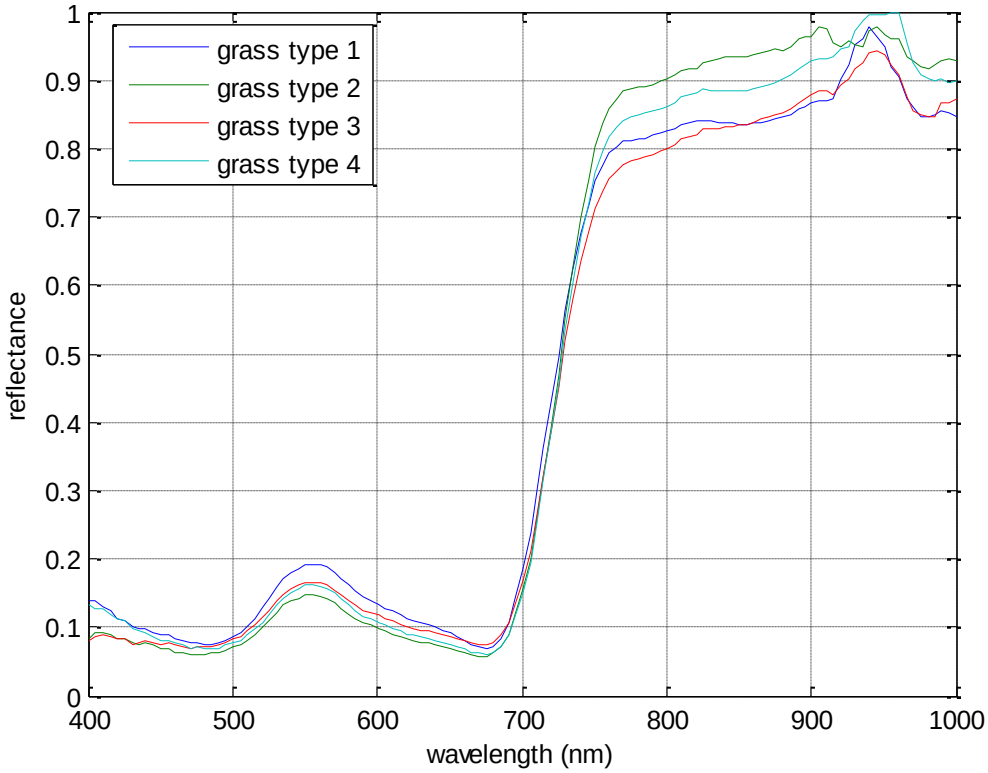

Fig. 6.20. Reflectance graphs for observed points in Fig. 3.22

As other observations, even in this case the work about GTI proceeds in the same way explained before, so it is necessary, through many experimental results, finding the threshold (here are necessary more thresholds because the goal is to discriminate between several kinds of grass). The total range could be 400 – 900 nm, and in 700 – 750 nm it is possible to look differences to understand types of grass. Another thing to say regards the precision of the threshold: in previously studied cases, differences from one type and the other (ill or healthy), was great in general; here is slighter, so even for having a good but not optimal classification, many observations are required.

6.11 – Considerations about number of observations

During the present chapter it was discussed how to use GTI method, and, joined with this, the importance of finding a good threshold for applying in useful way the algorithm. It was also said that there is not analytic way to obtain such threshold, so the only possible way of is trying and observing many times. But, how many times? And how memorize results to decide the threshold? Regarding the number, the best (and obvious), rule is to consider all the available

tries; but, for cases previously analyzed, about 1000 analyzed pixels were sufficient for finding a good threshold value. Talking now about 'how', it was followed the following strategy:

- Starting from ground references, memorization of a good number of local growths for every category
- Find maximum and minimum values for each category
- Find average values between ranges [29]

Consider this example: in order to detect ill plants of specie x there were considered about 1000 ground references for elements with disease and 1000 for healthy elements. Memorized all values of local growths (based on reflectance shape), it was possible finding these ranges:

- Healthy between 0.7 and 0.8
- Ill between 0.5 and 0.6

So, in this case there are only two categories and therefore it was necessary only one threshold in the middle of two intervals, exactly 0.65.

It could be possible having intervals like:

- Healthy between 0.6 and 0.7
- Ill between 0.55 and 0.65

In this case ranges were not separated so it was impossible to act like the previous example. A good (even if in general less accurate), way of proceeding was computing average for each interval (in the present case, respectively, 0.65 and 0.6), and then, the average for found numbers to obtain threshold (here 0.625). Cases like the last treated were very rare; in general it was possible finds separate intervals.

An analytic representation of what was above presented:

With 2 separated ranges, 1 and 2, the first below (that is with minor values) than the other one

$$M_1 = max_1 \quad (18)$$

$$M_2 = min_2 \quad (19)$$

$$\theta_{1,2} = \frac{(M_1 + M_2)}{2} \quad (20)$$

If ranges are not separated, M_1 and M_2 are different:

$$M_1 = \frac{max_1 + min_1}{2} \quad (21)$$

$$M_2 = \frac{max_2 + min_2}{2} \quad (22)$$

Where M_i is the chosen element among observed ones for range i-th, max_i and min_i are respectively maximum and minimum elements observed for i-th range and $\theta_{i,j}$ is the threshold between ranges i and j.

7 – Dynamic GTI

Improvements resulting from Static GTI are not sufficient, particularly for not-optimized images. Thus, a new method able to dynamically adapt to the images it was created.

7.1 – Introduction

During previous sections of this document it was always emphasized the contrast between reflectance optimized images and not optimized images, (also showing with examples the differences between these two approaches). All pictures analyzed before, even if not optimal from reflectance point of view, were optimal (or almost), from brightness, solar and atmospheric points of view (as seen before, with optimization steps it is possible to attenuate disturbing effects but not completely eliminate them). Unfortunately, ugly images are quite common and the approach described in Chapter 6 is reliable with good quality images but not always with others. In order to permit to GTI to be more general as possible, it was developed another approach, based on GTI idea, but reliable for all kinds of images by adapting to them in dynamic way (from here the idea to call this approach Dynamic GTI), by comparing results with NWI and mostly looking at the behavior of a lot of reflectance shapes.

7.2 – Low quality images

Below (Fig. 7.1), it is possible to see an example of low quality image (low-altitude), captured during the beginning of December 2007 is Suzukakedai, an area closed to Yokohama, Japan. With a simple eye observation is possible to see that the image is very dark, so it is so difficult to detect without instruments wilt areas. In this case, there is also the problem of autumnal leaves (because of the period), so every type of classification is very difficult. Images like that present a very irregular reflectance characteristic and the calibration method described in Chapter 3 is not enough to obtain a good reflectance. So for improving the shape it was used a 2^{nd} degree polynomial smoothing function, obtaining, for one pixel, graphs like Fig. 7.2:

Fig. 7.1. Low quality image regarding an oak tree forest

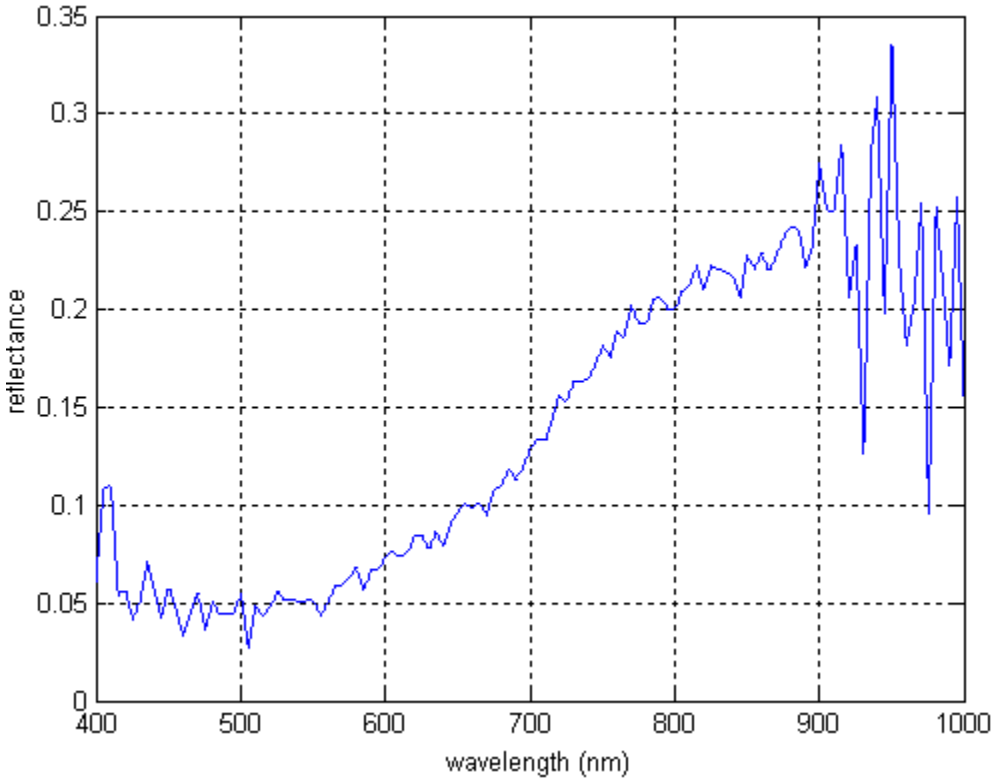

Fig. 7.2. Pixel – reflectance characteristic for low quality images

Nevertheless, the image is not very regular but presents trends which can be exploited. Using higher degree polynomial does not significantly improve results and takes too much time, so this is the best compromise. This smoothing uses a different set of precomputed coefficients popular in the field of chemistry. It is a type of Least Squares Polynomial smoothing. The amount of smoothing is controlled by two parameters: the polynomial order and the number of points used to compute each smoothed output value, in this case equal to 5. In general a smoothing function removes short-term variations, or noise to reveal the important underlying unadulterated form of the data.

7.3 – Refinement of total growth and ratios definitions

Looking at Fig. 7.2, it is possible noting that in intervals [400, 500] and [800, 900], the shape is particularly unstable, moreover in the calculus of total growth taking simply maximum and minimum values is not a good choice. Here is proposed an alternative method to catch reliable values, in particular the steps are:

- Mean values in [400 , 450]= μ_1 (23)

- Mean values in [450 , 500] = μ_2 (24)
- $S_1 = \min(\mu_1, \mu_2)$ (25)
- Mean values in [800 , 850]= μ_3 (26)
- Mean values in [850 , 900] = μ_4 (27)
- $S_2 = \max(\mu_3, \mu_4)$ (28)
- $total\ growth = S_2 - S_1$ (29)

In this way values are more robust and it is possible to get high quality results. Regarding local and autumnal growth, in their intervals at least the trend was understandable in all viewed images, so the procedures explained in Chapter 6 are still good.

So, it was possible defining characteristics below:

Def. 7.1. $local\ ratio$ is the ratio between local growth and total growth

Def. 7.2. $autumnal\ ratio$ is the ratio between autumnal growth and total growth

7.4 – Categories catcher algorithm

The clustering algorithm [6, 16, 17, 18, 19, 20, 21, 22, 23, 24, 28] here proposed (CC – categories catcher), represents an alternative to static threshold discrimination used in the previous chapter. It is able to divide a set of values into 2 different sets based on distances among coefficients, without knowing other information. This way of aging is particularly powerful for the work here discussed. To explain how it works is better to use an example (with an explanation of the algorithm before).

The set of numbers is I ={1, 2, 6, 4, 9} (in studied case I is the set of local ratios for each considered pixel). These values represent two different characteristics of something (a plant, animal or some phenomena for example). $I(i)$ is the i-th element of I.

The 2 sets in which breaking I are MAX and MIN, with the meaning of names that it will be clear soon. The algorithm is the following:

- ***Input***: $Initial\ vector\ of\ values\ I$
- ***Output***: Subsets into MIN and MAX vectors
- $MAX = \max(\{I(1), I(2)\}) = peak_2$
- $MIN = \min(\{I(1), I(2)\}) = peak_1$
- *//if* $I(1) = I(2)$ *are considered* $I(1)$ *and* $I(3)$ *(or other values in the set if these 2 are still equal). //Here there is the case in which* $I(1) \neq I(2)$.
- $diff = |peak_1 - peak_2|$
- ***for*** $i = 2 : |I|$
- $flag = 0$
    - ***if*** $(\left|\left(I(i+1) - peak_1\right)\right| \leq diff\ or\ \left|\left(I(i+1) - peak_2\right)\right| \leq diff)$
        - ***then***
        - $flag = 1$
        - ***if*** $(\left|\left(I(i+1) - peak_2\right)\right| \leq \left|\left(I(i+1) - peak_1\right)\right|)$
        - ***then***
            - add $I(i+1)$ to MAX otherwise to MIN
        - ***endif***
    - ***endif***
    - ***if*** $((flag == 0)$
        - ***then***
        - ***if*** $(\left|\left(I(i+1) - peak_2\right)\right| \geq \left|\left(I(i+1) - peak_1\right)\right|)$
        - ***then***
            - $MAX = MAX \cup MIN$
            - $MIN = \{I(i+1)\}$
        - ***else***
            - $MIN = MAX \cup MIN$
            - $MAX = \{I(i+1)\}$
        - ***endif***
    - ***endif***
    - ***if*** $(\max(MIN) \geq \max(MAX))$
    - ***then***
        - $peak_1 = average(MIN)$
        - $peak_2 = average(MAX)$
    - ***else***
        - $peak_2 = average(MIN)$
        - $peak_1 = average(MAX)$
    - ***endif***
    - $diff = |peak_1 - peak_2|$
    - $i = i + 1$
- ***endloop***

After the application of this algorithm, there are 2 sets, MAX and MIN that contain values of I ($I \equiv MAX \cup MIN$). Sometimes happens that some values of subset MAX (or MIN), are

comprised between maximum and minimum values of the other subset. In this case is simple correcting subsets moving elements. This method is an experimental division, so even if some value at the end is not in the right subset, minimal and maximal values of MAX and MIN found before are already very good ranges. For the set I introduced before, $MAX = \{6, 9\}$ and $MIN = \{1, 2, 4\}$ without adjustments at the end. From considerations done in Chapter 3, MAX and MIN represent healthy and wilt pixels respectively. Considering constant the execution time of conditional and assignment instructions, the complexity of CC is *O(I-1).*

As said before, the set is partitioned without giving parameters (like a threshold). In this way at the end there are 2 sets, but, what can we do if the purpose is splitting the initial set in four parts (like with grass species)? A good approach is applying a waterfall CC for every subset, that is obtaining for each MAX and MIN another couple of MAX and MIN until the number of wanted categories is reached. If the number of categories is odd, depending of subset range values, the experience or some tries should suggest which subset should be divide into 2 parts or what other strategy to follow. Coming back to CC features, $average(min(MAX), max(MIN))$, is always different (for every set of pixels analyzed), but this elastic behavior permits a better adaptation with low quality images. Below (Fig. 7.3), an example of division with CC for a set is depicted.

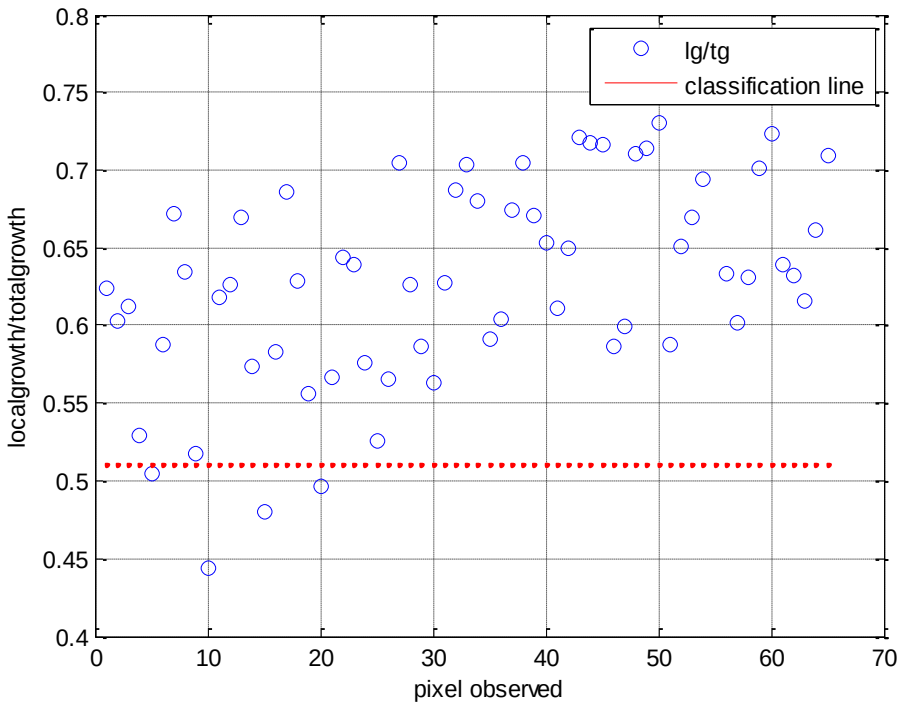

Fig. 7.3. CC division of a set of values

Classification line is $average(min(MAX), max(MIN))$. This value was not calculated by CC but is useful to observe division between subsets.

In general, applying normal GTI (with static threshold), results are in a lot of cases good, but, as said before, the static threshold may create problem in adapting to images and sometimes categorization is not very accurate. However, GTI remains a very good method and it can represent a base point of the study even for low quality images (using new way of calculating total growth).

7.5 – Threshold based corrections

As viewed, all work discussed in Chapter 3, it is still useful for applying CC to high quality images, because the thresholds found are a good starting point for refining subsets and, also regarding the autumnal problem, the threshold approach can provide a very good help. In particular, $average(min(MAX), \max(MIN))$ is an experimental threshold; from the study with high quality image, for oak trees it was found 0.6 as good fixed and theoretical threshold. So it is possible to correct division made by CC in this way:

$$if\ (average(min(MAX), \max(MIN)) > 0.6) \Rightarrow newaverage = average(min(MAX), \max(MIN)) - offset \quad (30)$$

$$if\ (average(min(MAX), \max(MIN)) < 0.6) \Rightarrow newaverage = average(min(MAX), \max(MIN)) + offset \quad (31)$$

A good offset value for oak trees is 0.1. In this way is possible a further improvement at subsets moving the division range (and therefore some elements of subsets), for arriving not far from the theoretical threshold. Obviously, even in this case, $newaverage$ will be always different but with a better adaptation than before. So, if for example the old average is 0.4, the new one will be 0.5 and each value of a subset between 0.4 and 0.5 will be moved in the other subset (in this case the greater one).

Regarding autumn, it is possible doing a very reliable comparison before applying CC (for both low and high quality images). If the autumnal ratio (valid also for low quality images because in that range of wavelengths the trend is maintained), is greater than the theoretical autumnal threshold showed in Chapter 3 (for oak trees is 0.15) and it is true also the other test explained in paragraph 6.3 (regarding autumnal concavity), than the considered pixel is stored into a new set and, at the end of CC algorithm, this set is directly moved into MAX set because healthy. Otherwise CC will be applied for that pixel.

CC always divides a set into two parts. So, if for example the considered area of pixel is all healthy, it will be divided into two parts. But, how to interpret this behavior? Knowing theoretical threshold values, it will be possible noting a great distance (even after the correction seen before), between it and the experimental threshold so it can arise some suspect about found

results. But this division can still reveal some interesting information, as explained in the following example. A plant not wilt now could be affected soon and its reflectance shape is evolving from healthy to wilt characteristic. So, CC division can be a good starting point in this case for discriminating between strongly healthy plants and possible wilt in near future ones. So it could be possible a prevention.

7.6 – MCC algorithm

A better alternative to CC algorithm saw before is another clustering-approach method, in particular was developed another algorithm, MCC (Multiple CC), which is able to divide a set *I* of values into a number of subsets less or equal to the length of *I*.

Below it is proposed the pseudocode of MCC; *I* is the initial set and *subset* is a matrix containing, for each row, a subset of *I:*

- ***Input***: Initial set of values *I*
- ***Output***: Subsets into *subset* matrix variable
- $range = \max(I) - \min(I)$
- $num = \|I\|$
- $subset(1{:}\,\|I\|, 1{:}\,num) = 0$ // *initial covering of subset matrix*
- ***for*** *i= 1 : num*
  - $subset(1, i) = i * (\frac{range}{num})$
- ***endloop***
- ***for*** $i = 1{:}\ \|I\|$
  - Each element of *I* is inserted into one row of subset. In particular it's chosen the row based on the smallest difference between the element of *I* and the first element of each row
- ***endloop***
- ***for*** $i = 1 :\ num\text{-}1$
  - for each row i of subset (without considering the first element and elements equal to 0), it's calculated the mean and, for every other row j of subset such that $\left|\text{mean}_i - \text{mean}_j\right| \leq \frac{\text{range}}{\text{num}}$ elements of the j-th row are moved into the i-th row of subset together with already existing ones
- ***endloop***

$|I|$ is the length of set *I*, *num* is the maximum number of subsets, here was imposed equal to the length of the initial set. For each iteration, the algorithm modifies *subset* matrix moving values from one row to another. In the end, only rows containing elements different from 0 will be subsets, the others can be discarded. If into the initial set appears value 0, as initial covering of *subset* matrix it is necessary another value that does not appear in the set. Imposing, for example, *num* equal to 2, there will be at most 2 subsets, and this can be a good choice for studying oak

trees. MCC is in general slower than K-means but for problems like the one here debated the K-means is not suitable. In fact K-means imposes to fix a rigid number of sets while MCC permits to fix just a maximum number. More precisely MCC can be considered of complexity equal to *O(I num)*

In general this algorithm is useful when it is unknown in advance how many categories there are. So, it is more general because permits a classification in a free number of subsets. For example, if the object of study is a grass field with an unknown number of different species, MCC can be the right choice for the work. Like CC, MCC preserves the following properties:

- $I \equiv \bigcup_{i=1}^{n} s_i$ with *I* the initial set, *n* the number of found subsets and s_i a subset
- $s_i \cap s_j \equiv \emptyset, i \neq j$

As an example of MCC working, if *I*={1, 4, 5, 66, 32, 78}, with *num* = 2, the set will be divided into 2 subsets, respectively {1, 4, 5, 32} and {66, 78}.

In the same conditions as paragraph 6.7, the time needed to analyze 500 pixels is about 6 minutes. Another interesting point of view of MCC can be explained through an example: the target of the study is discriminating between wilt and healthy oaks and it is used MCC with *num* equal to 10. The set *I* composed by, like in simple CC, *local ratio* for each pixel. At the end of algorithm running, *I* is divided into 5 subsets. At this point is possible assigning a coefficient to each one between 0 and 1 which can be viewed as "healthy index", so, for the subset with the highest values is 1 and is 0 for the lowest subset. Regarding the others, it is possible a linear assignment like, in growing order, 0.25, 0.50 and 0.75. This "fuzzy" approach has a precise meaning: if "healthy index" is 0 or 1, practically there is the certainty of the obtained results, instead for intermediate values there is a weighted uncertainty (which however in general gives an idea), and this is reasonable due to the experimental nature of method proposed. This way of observing subsets is better than a rigid categorization in which elements very close could belong to two totally different subsets. Therefore, this way of acting gives more reasonable results. Another thing to say is that, the more *num* is high the more subsets could be created, so with more "fuzzy sets". Making a comparison between CC and MCC, in general it is possible to observe a better behavior of the second one. So even in the case of known number of existing subsets, using MCC the final result is more reliable. Below (Fig. 7.4), there is an example of MCC running with an AISA not-optimized image regarding oak trees. Moreover, concerning fuzzy interpretation, Fig. 7.5 shows a possible mapping of an area of oak trees. Cheering results were obtained even for rice and grass fields as for Static GTI.

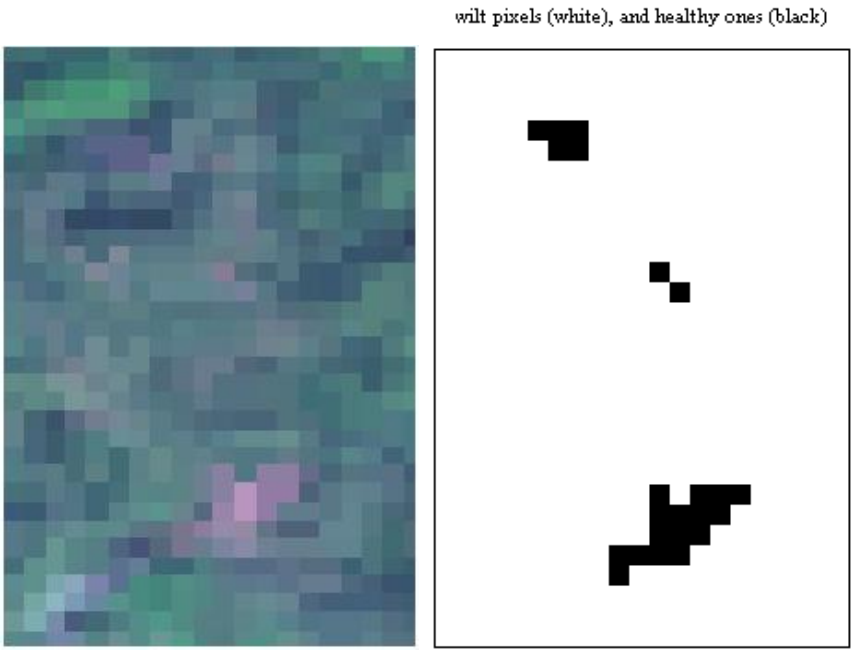

Fig. 7.4. Example of MCC

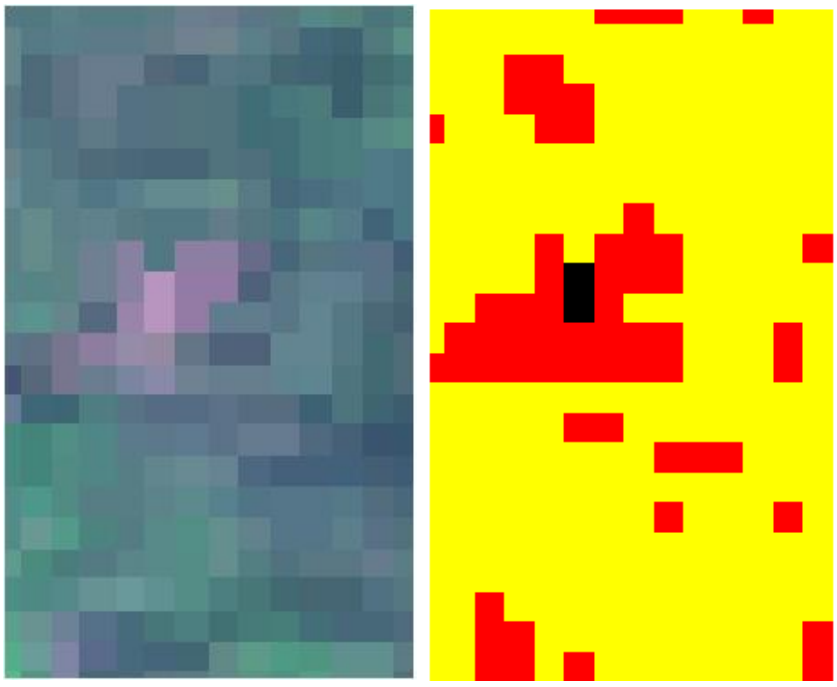

Fig. 7.5. Example of MCC with at most 4 subsets. A possible interpretation is: yellow areas affected at 0%, red ones at 50% and black at 100%

8 – Conclusions and future work

In this Chapter is shown a summary of reached results and future developments.

8.1 – Final considerations

As explained in Chapters 4 and 5, ANNs approach is not reliable for this study because of the high uncertainty of results and computational effort.
On the contrary, Static GTI method is very good for images captured in optimal conditions and Dynamic one can be used with good results for both optimal and not-optimal images. This result was clear observing the behavior of the method for different kinds of images. About optimal pictures, the result was compared with the one obtained with the Static GTI and in all cases the differences were really small; obviously for bad images Static GTI showed weakness in precision of classification. Precisely, to evaluate the quality of Static and Dynamic GTI, it was used the procedure explained below. There were considered oak trees pictures of different areas with known state (from human observations), of all pixels and for each of them, there were applied the two methods. For not-optimized images, Dynamic GTI (using MCC with *num* = 2), was able to individuate about 10% wilt pixels more than Static one. Moreover, respect to the known state, with Dynamic GTI, 96% of wilt pixels were detected and healthy pixels detected as wilt were almost absent. With optimal images, the error percentage of both method was very low. Obviously, GTI cannot be perfect but quality of results is high, so it is possible to obtain information about areas studied with a very good precision. It is important to say that computational effort is bigger for Dynamic GTI because of MCC (or CC), but the latter takes less time than ANNs. Regarding quality of methods, hundreds of different images were analyzed with good results so this kind of approach appears reliable. The table below (Fig. 8.1), summarizes data written above. Moreover, good results were reached applying GTI (Static and Dynamic), also for rice and grass fields. The approach followed was the same (Static and Dynamic GTI applied to pixels) but the number of observed pixels was not big. To have a reliable result to analyze, more images about rice and grass are necessary. Future research can go in this direction.
Moreover, every time autumnal filter was applied, errors were almost absent.

	ANNs	**Static GTI**	**CC**	**MCC (*num=2*)**
Not-optimal	60	85	95	96
Optimal	70	90	97	≈100

Fig. 8.1. Proximate percentage of success in pixel classification for the proposed methods

8.2 – How to improve detection

After the explanation of problems and ways of solving during all the present document, it is now useful to fix some base points in order to understand how is possible improving the work. It is a good choice dividing in two categories the exposition: hardware and software.

Regarding hardware, the best choice is suggested by the problem. For necessity of good details in observations not continuously, airborne images are the right choice; for the contrary it is good using satellite images. Regarding cases between these two above discussed, it is has to be find a good trade-off, so there are no some optimal rules in general but it is compulsory analyzing case by case.

Regarding both airborne and satellite instruments it is important to say that improvements in technology are present all years, therefore, soon, it could be possible having for example satellite images with spatial and spectrum resolution like nowadays airborne ones.

Talking about software, memorization of values with a large number of decimal digits is a good choice to improve precision even if there's the problem of memory space; but, about GTI for instance, the very important thing to improve for each vegetal specie is the threshold or way of classification. This is the element which, with a good hardware behind, represents the real discriminating element. But, as viewed in Chapters 3 and 4, also a good but not optimal threshold sometimes can be sufficient to determine at least macroscopic areas with a certain disease.

8.3 – An Italian project

The ASI (Agenzia Spaziale Italiana) [30], is developing PRISMA (PRecursore IperSpettrale of the Application Mission), a satellite for earth observation with hyperspectral sensor and a panchromatic, medium-resolution camera. In this way is simple capturing geometrical and structural information regarding areas observed.

Targets of mission are the following:

- Carry on an Italian mission for monitoring natural resources
- Make available in small time data regarding hyperpectral images
- Evaluating quality of observation from satellite

Technical features are:

- Spectrum range: 400 - 2500 nm
- Resolution of spectrum wavelengths captured: 10 nm

- Number of bands: 210
- Samples: 324
- From altitude of 700 km the spatial resolution along the track is between 20 and 30 m

Because of the greater distance from ground and problems connecting with its position (outside of the atmosphere), respect to instruments explained in paragraph 3.1, this device is less precise but has some advantages, like the possibility of capturing bigger areas and mostly a continuous observation. Below (Figs. 8.2a and 8.2b), is possible to see images regarding PRISMA.

Fig. 8.2. (a) (b) PRISMA satellite mock-up

Appendix

Apx. 1 - Platypus quercivorus

Platypus quercivorus (Apx. Fig. 1) attacks trees in tropical and temperate areas of the world. It is action on trunks is to block the flow of chlorophyll in direction of leaves from the end of June, approximately. Leaves of attacked trees, in two or three weeks at most will die.

Apx. Fig. 1. A Platypus quercivorus

Apx. 2 - Reflectance

In reflected light spectroscopy, the fundamental property that we want to obtain is spectral reflectance, that is the ratio between the reflected energy and the incident energy as a function of wavelength (it can assume values from 0 to 1), also possible to view as the ratio between radiance and illumination (for example the solar one). Energy at certain wavelengths is absorbed at different degrees from material to material and this can be useful for the identification. Big deflections of the spectral curves mark the wavelength ranges for which the material selectively absorbs the incident energy.

In plants, in the visible portion of the spectrum, the curve shape is governed by absorption effects from chlorophyll and other leaf pigments. Chlorophyll absorbs visible light very effectively but absorbs blue and red wavelengths more strongly than green, producing a characteristic small reflectance peak within the green wavelength range. This is why plants appear green to us. Reflectance rises sharply across the boundary between red and infrared wavelengths (from 40% to 50% for most plants). Here the curve shape is mostly due to the cell structure. Beyond 1.3 μm (middle infrared), reflectance decreases.

It is interesting to note that at the end of growing period, near infrared reflectance decreases and red reflectance increases, so It is possible to distinguish colors of autumn.

Reflectance varies between different types of vegetation, and also between different stress of same plants, so these data can be used for identification of different plants but also for detecting ill ones.

In order to study some phenomena, it is also possible having access to public library of images and graphs, such as the Aster Spectral Library, made available by NASA.

It is also very important to note that the spectral reflectance is only one factor of spectral radiance (the amount of reflected light reaching the sensor). Therefore, radiance depends not only from reflectance but also from the spectrum of the input solar energy, interactions of this energy during its downward and upward passages through atmosphere, the geometry of illumination for individual areas on the ground, and characteristics of the sensor system. All these things introduce a lot of problem in retrieval accurate spectral reflectance.

Apx. 3 - Spatial resolution

An imaging spectrometer makes spectral measurements of many small patches of the Earth's surface, each of which is represented as a pixel in the hyperspectral image. The size of the area represented by a single set of measurements defines the resolution. Possible values of this characteristic may be 20 m or 4 m depending also from the altitude (this means the an instrument can work at different resolutions because it can be at more diverse altitudes).

When the resolution is not refined, in many occasion two or more materials contribute to an individual spectrum measure, so the result is a mixed spectrum. Each contribute is called endmember spectrum.

There are two types of spectral mixtures: macroscopic or intimate.

In the first type, each photon interacts with only one material, so the energy reflected from the materials combines additively and each contribution to the composite spectrum is directly proportional to its area within the pixel.

In an intimate mixture, a single photon interacts with more than one material. This is the most difficult situation to manage, because, obviously the mixture are nonlinear.

Apx. 4 - Illumination factors

It is necessary to understand with a good precision by measurement, good assumptions or indirect computations, the spectrum of incoming solar energy. But that's not enough, because the amount of energy reflected by an area on the ground depends also on the angle on incidence, that

is the angle between the path of the incoming energy and a line perpendicular to the ground surface. The mathematical description is the following:

$$E_g = E_0 cos\theta \qquad \text{(A. 1)}$$

Where E_g is received energy at each wavelength, E_0 is the amount of incoming energy and θ is the angle of incidence. So, depending on day phases and season the energy varies. Also, if the ground is not flat there are variations.

Another important factor is shadow: clouds, trees, crop rows and many other objects can affect measurements for one or more adjacent pixels.

Apx. 5 - Effects from atmosphere and sensors

All types of atmosphere interact with incoming and reflected solar energy. It is possible to have reduction in these two types of energy. This is due to the adsorption by certain gases and by scattering by gas molecules. For example, water and carbon dioxide reduce incident and reflected energy almost completely in some wavelengths (1.4 and 1.9 μm), so analysis in these bands is very difficult and surely not very precise.

Another important and annoying effect is light scattered upward by the atmosphere which is added the radiance measured by the sensor in the visible and near infrared. This phenomena is called path radiance.

Sensors convert detected radiance in each wavelength channel to an electric signal which is scaled and quantized into discrete integer values. Different detectors produce different values and in general this phase of the work leads to loss in precision.

Apx. 6 - Reflectance conversion (a general vision)

To convert radiance to reflectance, in general, it is necessary to take into account some effects like solar ones, lighting effects due to sun angle and topography, atmospheric transmission, sensor gain and offset (internal instrument noise), and path radiance due to atmospheric scattering. In order to do conversions, there are two main different approaches: the first uses only information present on the image, and the second pay also attention on atmospheric condition and surface reflectance at the time the image was acquired.

Apx. 7 – Topographic reflectance correction

Starting from radiance values of hyperspectral images, is possible to obtain optimized reflectance values using a linear regression model like the one illustrated below:

$$L_H = L_T - \cos(i)m - b + \overline{L_T} \quad \text{(A. 2)}$$

Where, L_H is radiance observed for horizontal surface, L_T is radiance observed over slope terrain, $\overline{L_T}$ is the average radiance of L_T for forest pixels or other specific cover types in a scene of image, i is the sun incidence angle in relation to the normal of a pixel, and m and b are the slope and intercept of the regression line, respectively. This method is very good for removing slope influence. The target, moreover, is to remove all topographically induced illumination variations.

Apx. 8 – Rice blast

Magnaporthe grisea, also known as Rice blast fungus is a plant – pathogenic fungus that causes an important disease regarding rice but also other cereals like, for example, wheat and rye.
Below there is an image of dangerous parts of this fungus (Apx. Fig. 2):

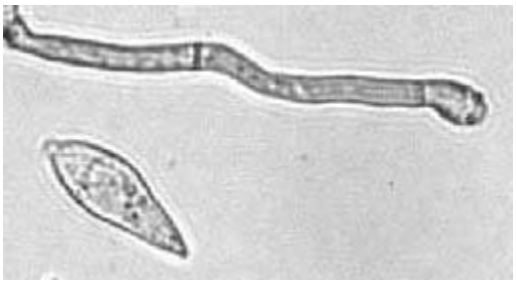

Apx. Fig. 2. A spore (conidium, produced asexually), and a conidiogenous cell of Magnaporthe grisea (that promotes production of spores in fungus)

This disease is present in 85 different countries and, every year, destroys enough rice to feed 60 million people. It is able to reproduce both sexually and asexually to produce specialized infectious known as Appressoria that infect aerial tissues and Hyphae that can affect root tissues.

Bibliography

[1] D. A. Landgrebe, "Signal Theory Methods in Multispectral Remote Sensing", John Wiley, Hoboken, NJ, 2003.

[2] K.S. Lee, D.H. Lee, K.A. Sudduth, S.O. Chung, N.R. Kitchen., S.T. Drummond, "Wavelength identification and diffuse reflectance estimation for surface and profile soil properties", Transactions of the ASABE, vol. 52(3), pp. 683-695, 2009.

[3] M.R. Nanni, J.A. Dematte, "Spectral reflectance methodology in comparison to traditional soil analysis", Soil Science Society of America Journal, vol. 70, pp. 393-407, 2006.

[4] Kuniaki Uto, Yuji Takabayashi, Yukio Kosugi,Toshinari Ogata, "Hyperspectral analysis of Japanese Oak wilt to determine normalized wilt index", Geoscience and Remote Sensing Symposium, 2008. IGARSS 2008 © IEEE International 07/2008,vol.2, p. II-295 – II-298.

[5] S.T. Monteiro, Y. Minekawa, Y. Kosugi, T. Akazawa, and K. Oda, "Prediction of sweetness and amino acid content in soybean crops from hyperspectral imagery", ISPRS Journal of Photogrammetry and Remote Sensing, vol. 62, no. 1, pp. 2–12, May 2007.

[6] Yukio Kosugi, Desjardins Guillaume, Yuji Takabayashi, Sildomar Takahashi Monteiro, Makoto Yamaki, Kuniaki Uto, Genya Saito, "Low-Altitude Hyperspectral Imaging of Naruko Integrated Field for the Interpretation of High – Altitude Observations", Symposium on Integrated Field Science, p. A-2, Sendai, Japan, 2008.

[7] Y. Minekawa, K. Uto, N. Kosaka, Y. Kosugi, H. Ando, Y. Sasaki, K. Oda, S. Mori, and G. Saito, "Salt-damaged paddy fields analyses using high-spatial-resolution hyper- spectral imaging system," in Proc. IEEE International Symposim on Geoscience and Remote Sensing, July 2005, vol. 3, pp. 2153–2156.

[8] Thomas Villmann, Erzs´ebet Mer´enyi, and Udo Seiffert, "Machine learning approaches and pattern recognition for spectral data," in Proceedings of the 16th European Symposium on Artificial Neural Networks ESANN 2008, Michel Verleysen, Ed., Evere, Belgium, 2008, pp. 433–444, D-Side Publications.

[9] Y. Minekawa, T. Edanaga, K. Uto, Y. Kosugi, and K. Oda, "Development of a low-altitude hyperspectral imaging system for measuring ground truth in agricultural fields," in Proc. IEEE International Symposim on Geoscience and Remote Sensing, July-Aug 2006, pp. 2052–2055.

[10] B. Krishnapuram, D. Williams, Y. Xue, A. Hartemink, L. Carin, and M. Figueiredo, “On semi-supervised classification”, in Proc. 18th Annual Conference on Neural Information Processing Systems, Vancouver, Canada, 2004.

[11] O. Chapelle, M. Chi, and A. Zien, “A continuation method for semisupervised svms”, in Proceedings of the 23rd International Conference on Machine Learning. 2006, pp. 185–192, ACM Press.

[12] Richard P. Lippmann, “An introduction to computing with neural nets,” IEEE ASSP Magazine, vol. 4, no. 87, pp. 4–23, 1987.

[13] Udo Seiffert, Lakhmi C. Jain, and Patrick Schweizer, Eds., “Bioinformatics using Computational Intelligence Paradigms”, vol. 176 of Studies in Fuzziness and Soft Computing, Springer-Verlag, Heidelberg, 2005.

[14] Udo Seiffert, Barbara Hammer, Samuel Kaski, and Thomas Villmann, “Neural networks and machine learning in bioinformatics – theory and applications,” in Proceedings of the 14th European Symposium on Artificial Neural Networks ESANN 2006, Michel Verleysen, Ed., Evere, Belgium, 2006, pp. 521–532, D-Side Publications.

[15] Thomas Martinetz and Klaus Schulten, “A Neural Gas learns topologies”, in Artificial Neural Networks, Teuvo Kohonen, Kai M¨akisara, Olli Simula, and Jari Kangas, Eds., pp. 397–402. North-Holland, Amsterdam, 1991.

[16] G. Camps-Valls and L. Bruzzone, “Kernel-based methods for hyperspectral image classification”, IEEE Transactions on Geoscience and Remote Sensing, vol. 43, pp. 1351–1362, 2005.

[17] A. Martinez-Uso, F. Pla, J. M. Sotoca, and P. Garcia-Sevilla, ”Clustering-based hyperspectral band selection using information measures”, IEEE Transactions on Geoscience and Remote Sensing, 45(12):4158–4171, Dec. 2007.

[18] A. Plaza, P. Martinez, R. Perez, and J. Plaza, “A quantitative and comparative analysis of endmember extraction algorithms from hyperspectral data”, IEEE Trans. Geosci. Remote Sens., vol. 42, no. 3, pp. 650–663, 2004.

[19] J. A. Benediktsson, J. A. Palmason, and J. R. Sveinsson, "Classification of hyperspectral data from urban areas based on extended morphological profiles", IEEE Transactions on Geoscience and Remote Sensing, vol. 43, pp. 480-491, 2005.

[20] G. Camps-Valls and L. Bruzzone, "Kernel-based methods for hyperspectral image classification", IEEE Transactions on Geoscience and Remote Sensing, vol. 43, pp. 1351-1362, Jun 2005.

[21] G. Camps-Valls, L. Gomez-Chova, J. Munoz-Mari, J. L. Rojo - Alvarez, and M. Martinez-Ramon, "Kernel-based framework for multitemporal and multisource remote sensing data classification and change detection", IEEE Transactions on Geoscience and Remote Sensing, vol. 46, pp. 1822-1835, Jun 2008.

[22] A. P. Schaum, ”Hyperspectral detection algorithms: From old ideas to operational concepts to next generation”, in Proceeding of 12th SPIE Conference on Algorithms and Technologies for Multispectral, Hyperspectral and Ultraspectral Imagery, vol. 6233, 623305, 2006.

[23] B Bue, B Csath´o, and E Mer´enyi, “Automated labeling of segmented hyperspectral imagery via spectral matching”, Proceedings IEEE WHISPERS 2009, Aug 2009.

[24] A. Martinez-Uso, F. Pia, J.M. Sotoca, P. Garcia-Sevilla, “Clustering-Based Hyperspectral Band Selection Using Information Measures”, Geoscience and Remote Sensing, © IEEE 12/2007, vol. 45 issue:12, p. 4158 – 4171.

[25] Meysam Argany, Jalai Amini, M. Reza Saradjian, “Artificial neural networks for improvement of classification accuracy in Landsat ETM+ images”, GIS development, Map Middle East 2006.

[26] Ruiliang Pu, Maggi Kelly, Gerald L. Anderson, Peng Gong, “Using CASI Hyperspectral Imagery to Detect Mortality and Vegetation Stress Associated with a New Hardwood Forest Disease”, Photogrammetric Engineering & Remote Sensing, January 2008.

[27] L. Bousquet, S. Lacherade, S. Jacquemoud, and I. Moya, “Leaf measurements and model for specular and diffuse components differentiation”, Remote Sensing of Environment, vol. 98, no. 2-3, pp. 201–211, October 2005.

[28] G. McLachlan and D. Peel, “Finite Mixture Models”, Wiley series in probability and mathematical statistics, John Wiley & Sons, Inc., 2000.

[29] Christopher M. Bishop, “Pattern Recognition and Machine Learning”, Springer 2006.

[30] http://www.asi.it